AD-A150 280 LIQUID MOMENT ON A FILLED CONING CYLINDER DURING 1/1
SPIN-UP: AD HOC MODEL(U) ARMY BALLISTIC RESEARCH LAB
ABERDEEN PROVING GROUND MD N GERBER DEC 84 BRL-TR-2628
UNCLASSIFIED SBI-AD-F300 562 F/G 19/1 NL

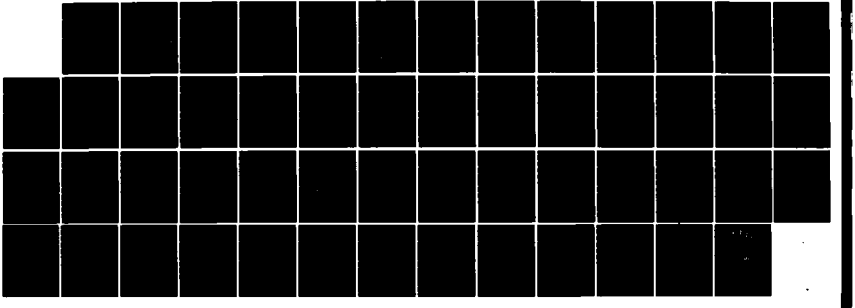

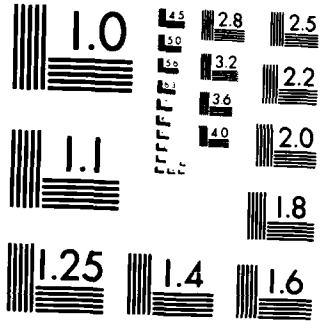

(12)

AD-A150 280

AD

BRL

TECHNICAL REPORT BRL-TR-2628

LIQUID MOMENT ON A FILLED CONING CYLINDER DURING SPIN-UP: AD HOC MODEL

Nathan Gerber

December 1984

US ARMY BALLISTIC RESEARCH LABORATORY
ABERDEEN PROVING GROUND, MARYLAND

Destroy this report when it is no longer needed.
Do not return it to the originator.

Additional copies of this report may be obtained from the National Technical Information Service, U. S. Department of Commerce, Springfield, Virginia 22161.

The findings in this report are not to be construed as an official Department of the Army position, unless so designated by other authorized documents.

The use of trade names or manufacturers' names in this report does not constitute indorsement of any commercial product.

UNCLASSIFIED

SECURITY CLASSIFICATION OF THIS PAGE (When Data Entered)

REPORT DOCUMENTATION PAGE	READ INSTRUCTIONS BEFORE COMPLETING FORM
1. REPORT NUMBER: TECHNICAL REPORT BRL-TR-2628	2. GOVT ACCESSION NO.: AD-A150 280
	3. RECIPIENT'S CATALOG NUMBER:
4. TITLE (and Subtitle): LIQUID MOMENT ON A FILLED CONING CYLINDER DURING SPIN-UP: AD HOC MODEL	5. TYPE OF REPORT & PERIOD COVERED: Final
	6. PERFORMING ORG. REPORT NUMBER:
7. AUTHOR(s): Nathan Gerber	8. CONTRACT OR GRANT NUMBER(s):
9. PERFORMING ORGANIZATION NAME AND ADDRESS: US Army Ballistic Research Laboratory, ATTN: AMXBR-LFD, Aberdeen Proving Ground, Maryland 21005-5066	10. PROGRAM ELEMENT, PROJECT, TASK AREA & WORK UNIT NUMBERS: RDT&E 1L161102AH43
11. CONTROLLING OFFICE NAME AND ADDRESS: US Army Ballistic Research Laboratory, ATTN: AMXBR-OD-ST, Aberdeen Proving Ground, Maryland 21005-5066	12. REPORT DATE: DECEMBER 1984
	13. NUMBER OF PAGES: 53
14. MONITORING AGENCY NAME & ADDRESS (if different from Controlling Office)	15. SECURITY CLASS. (of this report): UNCLASSIFIED
	15a. DECLASSIFICATION DOWNGRADING SCHEDULE

16. DISTRIBUTION STATEMENT (of this Report)

Approved for public release; distribution unlimited.

17. DISTRIBUTION STATEMENT (of the abstract entered in Block 20, if different from Report)

18. SUPPLEMENTARY NOTES

19. KEY WORDS (Continue on reverse side if necessary and identify by block number)

Linearized Navier-Stokes Equations	Liquid Payload
Liquid-Filled Shell	Liquid Spin-Up
Liquid Moment Coefficient	Resonance
Liquid Pressure Moment	Rotating Fluid
Liquid Viscous Shear Moment	Spinning Nutating Cylinder

20. ABSTRACT (Continue on reverse side if necessary and identify by block number) (bja)

A liquid-filled right circular cylinder, coning at constant frequency and small amplitude, impulsively begins spinning with a fixed angular velocity. The ensuing history of the moment, i.e., pressure plus viscous shear, exerted by the liquid on the container is investigated here by computation of the quasi-steady state response of the fluid to the motion of the shell. The

(continued)

DD FORM 1 JAN 73 1473 EDITION OF 1 NOV 65 IS OBSOLETE

UNCLASSIFIED

SECURITY CLASSIFICATION OF THIS PAGE (When Data Entered)

partial differential equations of flow are linearized, and a modal analysis (separated variable solution) is applied. The difficulty with endwall boundary conditions which arises from stipulating a modal analysis is avoided by specifying a heuristic boundary condition and then satisfying it approximately. The current procedure for approximating the boundary condition is an improvement over the one employed in previous work (ARBRL-TR-02563) to obtain the pressure moment. Calculations indicate that peaks of overturning moment occur at or near those times when the coning frequency is equal to one of the frequencies of inertial oscillations of the liquid. This phenomenon of resonance extends the results of Stewartson obtained for inviscid perturbations in solid body rotation. Included here also are a discussion of the accuracy of a part of the method and comparisons with output of the inviscid perturbation method and the above-mentioned previous method.

TABLE OF CONTENTS

LIST OF ILLUSTRATIONS

I. INTRODUCTION

This report deals with the forces and moments exerted by a liquid payload during spin-up on a spinning and nutating right circular cylinder. The current work stems from the original paper by Stewartson,[1] improved by the viscous correction of Wedemeyer.[2] It represents an extension of the work presented in Reference 3, which treats the particular case of circular angular motion with constant nutational frequency and zero yaw growth. Here we determine the viscous shear contribution to the moment in addition to that of the pressure. The ad hoc model of Murphy,[4] described in Reference 3, is employed to compute the spin-up moment.

In the analysis, two coordinate systems are considered. The first is an inertial system, the unyawed reference frame shown in Figure 1, in which cylindrical polar coordinates* (r, θ, x) and Cartesian coordinates (y, z, x) are used. The second coordinate system, used to describe the projectile motion, is the $\tilde{y}$, $\tilde{z}$, $\tilde{x}$ non-spinning system that has the $\tilde{x}$-axis along the projectile axis of symmetry; the $\tilde{y}$ and $\tilde{z}$ axes are omitted from Figure 1 for clarity. The $x = 0$ and $\tilde{x} = 0$ values are located at the midplanes of the unyawed and yawed cylinders, respectively. The $\tilde{x}$-axis is nutating about the x-axis with the angle $K_1(t)$; the pivot point lies at the midplane. The components of the projection in the y, z plane of a unit vector lying on the $\tilde{x}$-axis are denoted by n_{YE} and n_{ZE}, respectively. It is convenient to combine the two components of yaw into a single complex variable

$$\tilde{\xi} = -(n_{YE} + i\, n_{ZE}). \tag{1.1}$$

The nomenclature here is that prescribed in Reference 5 and used in References 3, 6, and 7.

---

*Definitions of quantities are given in the LIST OF SYMBOLS Section.

1. K. Stewartson, "On the Stability of a Spinning Top Containing Liquid," Journal of Fluid Mechanics, Vol. 5, Part 4, 1959.

2. E. H. Wedemeyer, "Viscous Corrections to Stewartson's Stability Criterion," Ballistic Research Laboratory, Aberdeen Proving Ground, Maryland, BRL Report No. 1287, June 1966. (AD 489687)

3. N. Gerber, "Contribution of Pressure to the Moment During Spin-Up on a Nutating Liquid-Filled Cylinder: Ad Hoc Model," Ballistic Research Laboratory, Aberdeen Proving Ground, Maryland, ARBRL-TR-02563, June 1984. (AD A143678)

4. C. H. Murphy, "Moment Induced by Liquid Payload During Spin-Up Without a Critical Layer," Ballistic Research Laboratory, Aberdeen Proving Ground, Maryland, ARBRL-TR-02581, August 1984. (AD A145716) (See also AIAA 22nd Aerospace Sciences Meeting, Reno, Nevada, AIAA Paper No. 84-0229, January 1984.)

The projectile motion is specified as

$$\tilde{\xi} = K_1 e^{i\phi_1} = K_0 e^{if\dot{\phi}t}, \tag{1.2}$$

where

$$K_1 = K_0 e^{\varepsilon\tau\dot{\phi}t}, \qquad \phi_1 = \tau\dot{\phi}t, \qquad f = (1 - i\varepsilon)\,\tau. \tag{1.3}$$

Here t is time, $\dot{\phi}$ (rad/s) is the axial component of the angular velocity of the cylinder; τ and $\varepsilon\tau$ are nutational frequency and yaw growth rate, respectively, divided by $\dot{\phi}$. K_0 is the magnitude of the yaw at time t = 0; ϕ_1 is the angular orientation of the $\tilde{x}$-axis in the y, z, x system as shown in Figure 1. Lengths and distances are non-dimensionalized by a, the cross-sectional radius of the cylinder. The yaw grows when $\varepsilon\tau > 0$; however, in this study we apply the restriction $\varepsilon = 0$.

Computational results will be presented in terms of time histories of non-dimensional moment coefficients. Each history is specified by the three parameters Re, $A \equiv c/a$, and τ, where

$$Re = a^2\dot{\phi}/\nu \tag{1.4}$$

is the Reynolds number and ν is the kinematic viscosity of the liquid. The reader is referred to References 3 and 7 for details of the analyses; only the relevant features will be repeated here.

II. FLOW PROBLEM

A. Flow Variables.

Here, as in previous work,[5,6,7] we assume the yaw to be sufficiently small so that a linearized analysis is applicable, i.e., the flow may be

---

5. *C. H. Murphy, "Angular Motion of a Spinning Projectile with a Viscous Liquid Payload," Ballistic Research Laboratory, Aberdeen Proving Ground, Maryland, ARBRL-MR-03194, August 1982. (AD A118676) (See also Journal of Guidance, Control, and Dynamics, Vol. 6, July-August 1983, pp. 280-286.)*

6. *N. Gerber, R. Sedney, and J. M. Bartos, "Pressure Moment on a Liquid-Filled Projectile: Solid Body Rotation," Ballistic Research Laboratory, Aberdeen Proving Ground, Maryland, ARBRL-TR-02422, October 1982. (AD A120567)*

7. *N. Gerber and R. Sedney, "Moment on a Liquid-Filled Spinning and Nutating Projectile: Solid Body Rotation," Ballistic Research Laboratory, Aberdeen Proving Ground, Maryland, ARBRL-TR-02470, February 1983. (AD A125332)*

considered the sum of a known basic unperturbed axisymmetric flow and a 3-D perturbation flow. The basic flow employed here is the Wedemeyer spin-up model[8] (see Eqs. (2.2) and (2.3) in Reference 3) which is obtained by finite difference calculations. Thus,

$$u = U(r, \dot{\phi}t) - K_0 \overset{*}{u}(r, \theta, x, \dot{\phi}t) \tag{2.1a}$$

$$v = V(r, \dot{\phi}t) - K_0 \overset{*}{v}(r, \theta, x, \dot{\phi}t) \tag{2.1b}$$

$$w = W(r, x, \dot{\phi}t) - K_0 \overset{*}{w}(r, \theta, x, \dot{\phi}t) \tag{2.1c}$$

$$p = P(r, \dot{\phi}t) - K_0 \overset{*}{p}(r, \theta, x, \dot{\phi}t). \tag{2.1d}$$

The u, v, w are velocity components in the radial, azimuthal, and axial directions, respectively; U, V, W are the corresponding velocity components of the basic flow. The velocity components of the perturbed flow are $\overset{*}{u}$, $\overset{*}{v}$, and $\overset{*}{w}$. The quantity p is pressure, P is the pressure of the basic flow, and $\overset{*}{p}$ is the perturbation pressure. Velocity is non-dimensionalized by $a\dot{\phi}$ and pressure by $\rho a^2 \dot{\phi}^2$, where ρ is the density of the liquid. The angular motion prescribed by Eq. (1.2) leads to boundary conditions on the perturbed velocity components at the sidewall and endwalls with a t, θ dependence of $e^{i(\tau\dot{\phi}t-\theta)}$.

B. Assumptions of Model.

The present model assumes the following form for the perturbed flow variables:

$$\overset{*}{u} = \text{Real}\left[\underline{u}(r, x; \dot{\phi}t) \exp\{i(\tau\dot{\phi}t-\theta)\}\right] \tag{2.2a}$$

$$\overset{*}{v} = \text{Real}\left[\underline{v}(r, x; \dot{\phi}t) \exp\{i(\tau\dot{\phi}t-\theta)\}\right] \tag{2.2b}$$

$$\overset{*}{w} = \text{Real}\left[\underline{w}(r, x; \dot{\phi}t) \exp\{i(\tau\dot{\phi}t-\theta)\}\right] \tag{2.2c}$$

$$\overset{*}{p} = \text{Real}\left[\underline{p}(r, x; \dot{\phi}t) \exp\{i(\tau\dot{\phi}t-\theta)\}\right]. \tag{2.2d}$$

---

8. E. H. Wedemeyer, "The Unsteady Flow Within a Spinning Cylinder," Ballistic Research Laboratory, Aberdeen Proving Ground, Maryland, BRL Report No. 1225, October 1963. (AD A431846) (See also Journal of Fluid Mechanics, Vol. 20, Part 3, 1964, pp. 383-399.)

The $\underline{u}$, $\underline{v}$, $\underline{w}$, and $\underline{p}$ are complex functions; the time, t, enters them only as a parameter due to the "quasi-steady" assumption (discussed at the end of Section II.A in Reference 3). The resulting problem in $\underline{u}$, $\underline{v}$, $\underline{w}$, and $\underline{p}$ is formally time-independent, implying that there are no transients in the lag between the motion of the cylinder and the corresponding response of the flow. The solution of Eq. (2.2) would be most valid late in the spin-up history of the fluid, and its applicability would be expected to decrease as t decreases.

The differential equations for $\underline{u}$, $\underline{v}$, $\underline{w}$, and $\underline{p}$ are given by Eq. (2.9) in Reference 3, the axis and sidewall boundary conditions by Eqs. (2.10) and (2.11) in the same report. $V(r)$ and $\partial V/\partial r$ occur in these, but U and W are absent.

The following ad hoc endwall boundary condition is applied in the absence of a rationally derived boundary condition:

$$L(\underline{w}) \equiv (1 \mp \delta c_E \, \partial/\partial x) \, \underline{w} = i \, (1 - \tau) \, r \qquad \text{at } x = \pm A. \tag{2.3}$$

It is discussed briefly in the last two paragraphs of Chapter I of Reference 3. This condition will not be satisfied exactly by the solution but only to within the accuracy of a least squares fit. The complex "thickness" δc_E is found as follows:

$$\alpha_E = 2^{-1/2} \, Re_E^{1/2} \, (1 - i) \, (3 - \tau)^{1/2} \tag{2.4a}$$

$$\beta_E = 2^{-1/2} \, Re_E^{1/2} \, (1 + i) \, (1 + \tau)^{1/2} \tag{2.4b}$$

$$\delta c_E = \left[\frac{1}{2\alpha_E} \left(1 - \frac{2}{1 - \tau}\right) + \frac{1}{2\beta_E} \left(1 + \frac{2}{1 - \tau}\right)\right], \tag{2.4c}$$

with the restriction $(3 - \tau) \geq 0$. The "effective" Reynolds number used here is given by

$$Re_E \, (t) = \left[2 \int_0^1 V \, (r; \dot{\phi}t) \, dr\right] Re. \tag{2.5}$$

For solid-body rotation, with $V = r$, the bracketed term is equal to unity, and $Re_E = Re$; while the fluid is spinning up, $V < r$ and $Re_E < Re$.

C. Flow Solution.

The flow solution is expressed as

$$\underline{u} = \hat{u}_0(r)\, x + \sum_{k=1}^{KF} \hat{u}_k(r) \sin \lambda_k x + \sum_{j=1}^{NJ} d_j\, \bar{u}_j(r) \sin \mu_j x \tag{2.6a}$$

$$\underline{v} = \hat{v}_0(r)\, x + \sum_{k=1}^{KF} \hat{v}_k(r) \sin \lambda_k x + \sum_{j=1}^{NJ} d_j\, \bar{v}_j(r) \sin \mu_j x \tag{2.6b}$$

$$\underline{w} = \hat{w}_0(r) - \sum_{k=1}^{KF} \hat{w}_k(r) \cos \lambda_k x - \sum_{j=1}^{NJ} d_j\, \bar{w}_j(r) \cos \mu_j x \tag{2.6c}$$

$$\underline{p} = \hat{p}_0(r)\, x + \sum_{k=1}^{KF} \hat{p}_k(r) \sin \lambda_k x + \sum_{j=1}^{NJ} d_j\, \bar{p}_j(r) \sin \mu_j x, \tag{2.6d}$$

where $\hat{u}_0$, $\hat{u}_k$, $\bar{u}_j$, etc. satisfy Eq. (2.23) of Reference 3.

The λ_k's are solutions to the functional equation (see Eq. (31) of Reference 6)

$$\cos \lambda_k A + \lambda_k\, \delta c_E \sin \lambda_k A = 0, \tag{2.7}$$

so that every $\hat{w}_k(r) \cos \lambda_k x$ term satisfies the homogeneous endwall condition $L(\hat{w}_k \cos \lambda_k x) = 0$ at $x = \pm A$, where the operator L is defined in Eq. (2.3). At $r = 1$, $\bar{u}_j = \bar{v}_j = \bar{w}_j = 0$, so that the μ_j's are eigenvalues of Eq. (2.23) of Reference 3 with λ_k replaced by μ_j. (The normalization of the corresponding eigenfunctions is described in Chapter III.C of Reference 9.) Thus, the partial solution taken from Eq. (2.6),

---

6. [illegible], Jr., [illegible], and [illegible], "Oscillation of a [illegible] [illegible]-Body Rotation," [illegible] Maryland, [illegible]

$$\underline{u}_\pi = \hat{u}_0(r)\, x + \sum_k \hat{u}_k(r) \sin \lambda_k x, \qquad \text{etc.,} \tag{2.8}$$

satisfies the sidewall conditions (Eq. (2.11) of Reference 3):

$$\underline{u}\,(r = 1) = \underline{u}_\pi\,(r = 1) = -\,i\,(1 - \tau)\,x \tag{2.9a}$$

$$\underline{v}\,(r = 1) = \underline{v}_\pi\,(r = 1) = -\,(V_r(r = 1) - \tau)\,x \tag{2.9b}$$

$$\underline{w}\,(r = 1) = \underline{w}_\pi\,(r = 1) = i\,(1 - \tau). \tag{2.9c}$$

Finally, the partial solution

$$\underline{u}_p = \hat{u}_0(r)\, x + \sum_j d_j\, \bar{u}_j(r) \sin \mu_j x \tag{2.10a}$$

$$\underline{w}_p = \hat{w}_0(r) - \sum_j d_j\, \bar{w}_j(r) \cos \mu_j x, \qquad \text{etc.,} \tag{2.10b}$$

is left to satisfy the non-homogeneous endwall boundary condition of Eq. (2.3). The $\underline{w}_p$ of Eq. (2.10b) cannot satisfy Eq. (2.3) identically; the *complex* d_j's are therefore determined so as to minimize in a least squares sense the error over the interval $0 \le r \le 1$.

D. Operational Procedure.

The current operational procedure differs from the one employed in Reference 3. The new method was suggested by C. H. Murphy. The first step is to calculate the complex eigenvalues μ_j and the eigenfunctions $\bar{u}_j$, $\bar{v}_j$, $\bar{w}_j$, $\bar{p}_j$ as before for $j = 1, \ldots, Nd$.

The next step is to solve the differential equations for $\hat{u}_0$, $\hat{v}_0$, $\hat{w}_0$, $\hat{p}_0$ (Eq. (2.23) of Reference 3, with $\lambda_k = 0$ and $\epsilon_p = 1$). The orthonormalization process of Reference 9 is employed to obtain three linearly independent continuous solutions $(\hat{u}_i, \hat{v}_i, \hat{w}_i, \hat{p}_i, \hat{v}_i', \hat{w}_i')$, where $i = 1, 2, 3$, by applying the following three independent sets of boundary conditions at $r = 1$:

$$\hat{u}_1(1) = 1, \qquad \hat{v}_1(1) = 0, \qquad \hat{w}_1(1) = 0 \tag{2.11a}$$

$$\hat{u}_2(1) = 0, \qquad \hat{v}_2(1) = 1, \qquad \hat{w}_2(1) = 0 \tag{2.11b}$$

$$\hat{U}_3(1) = -\frac{(1-\tau)}{(1+\tau)}, \qquad \hat{V}_3(1) = \frac{i\,(1-\tau)}{(1+\tau)}, \qquad \hat{W}_3(1) = 1. \tag{2.11c}$$

The third set, Eq. (2.11c), is $[i\,(1-\tau)]^{-1}$ times the boundary values of the particular solution for solid body rotation. In providing a known limiting case, these latter numbers prove to be helpful in checking the program and assessing the accuracy of the procedure. Finally,

$$\begin{aligned} \hat{u}_o &= k_1\,\hat{U}_1 + k_2\,\hat{U}_2 + k_3\,\hat{U}_3 \\ \hat{v}_o &= k_1\,\hat{V}_1 + k_2\,\hat{V}_2 + \hat{k}_3\,\hat{V}_3 \\ \hat{w}_o &= k_1\,\hat{W}_1 + k_2\,\hat{W}_2 + k_3\,\hat{W}_3, \quad \text{etc,} \end{aligned} \tag{2.12}$$

where k_1, k_2, and k_3 are constants to be determined.

We apply the same condition on $\hat{w}_o(1)$ as on $\underline{w}(1)$; namely, Eq. (2.9c):

$$\hat{w}_o(1) = i\,(1-\tau). \tag{2.13}$$

Then, by application of Eq. (2.11),

$$k_3 = i\,(1-\tau) \tag{2.14}$$

and

$$\hat{w}_o(r) = k_1\,\hat{W}_1(r) + k_2\,\hat{W}_2(r) + i\,(1-\tau)\,\hat{W}_3(r). \tag{2.15}$$

Upon substitution from Eq. (2.15) and Eq. (2.10b), the endwall ad hoc boundary condition at x = A becomes

$$R(r) = \psi(r) - \sum_{j=1}^{NJ+2} e_j\,\bar{w}_j(r) = 0, \tag{2.16}$$

where

$$e_j = (\cos\mu_j A + \delta c_E\,\mu_j \sin\mu_j A)\,d_j \qquad (j = 1,2,\ldots NJ) \tag{2.17a}$$

$$e_{NJ+1} = k_1, \qquad e_{NJ+2} = k_2 \tag{2.17b}$$

$$\bar{w}_{NJ+1} = -\hat{W}_1(r) \tag{2.17c}$$

$$\bar{w}_{NJ+2} = -\hat{W}_2(r) \tag{2.17d}$$

$$\psi(r) = i(1-\tau)[\hat{W}_3(r) - r]. \tag{2.17e}$$

The error, R(r), will not be identically zero. We seek to optimize the fit of the solution to the boundary condition by determining a set of e_j's which minimizes the error integral

$$g(e_1, \ldots, e_{NJ+2}) \equiv \int_0^1 |R(r)|^2 \, dr. \tag{2.18}$$

The procedure for calculating the e_j's is presented in Appendix A. There are now NJ + 2 functions and constants with which to minimize the error, as compared with NJ functions and constants in the method of Reference 3. This additional flexibility is expected, generally, to produce an improvement in accuracy in satisfying the endwall boundary condition. The measure of the relative error adopted here is given by

$$Er = [g / \int_0^1 |\psi(r)|^2 \, dr]^{1/2}. \tag{2.19}$$

The constants k_1, k_2, and k_3 are now evaluated from Eqs. (2.17b) and (2.14).

Finally, the differential equations (Eq. (2.23) of Reference 3 with $\varepsilon_p = 0$) are solved for $\hat{u}_k$, $\hat{v}_k$, $\hat{w}_k$, $\hat{p}_k$ with the boundary conditions at r = 1 obtained by subtracting $\hat{u}_o(1)x$, $\hat{v}_o(1)x$, $\hat{w}_o(1)$ from the conditions of Eq. (2.9). Thus for $k \neq 0$,

$$\hat{u}_k(1) = -[\hat{u}_o(1) + i(1-\tau)]\, b_k \tag{2.20a}$$

$$\hat{v}_k(1) = -[\hat{v}_o(1) + V_r(1) - \tau]\, b_k \tag{2.20b}$$

$$\hat{w}_k(1) = 0, \tag{2.20c}$$

where

$$b_k = \frac{(2/\lambda_k)^2 [1 + (\lambda_k \, \delta c_E)^2] \sin \lambda_k A}{A[1 + (\lambda_k \, \delta c_E)^2] - \delta c_E}, \tag{2.21}$$

given by Eq. (2.29) of Reference 3. The complete solution is now available to compute forces and moments.

III. LIQUID MOMENTS

A. Sidewall Moment.

Definitions of sidewall pressure and shear moment coefficients are stated in Eq. (5.6) of Reference 7. $M_{L\tilde{Z}L}$ is the moment about the (transverse) $\tilde{z}$ - axis exerted by the liquid on the sidewall of the container:

$$M_{L\tilde{Z}L}/(2\pi\rho a^4 c\ \dot{\phi}^2 \tau K_1) = C_{(LSM)PL} \sin \tau\dot{\phi}t + C_{(LIM)PL} \cos \tau\dot{\phi}t + C_{(LSM)VL} \sin \tau\dot{\phi}t + C_{(LIM)VL} \cos \tau\dot{\phi}t. \tag{3.1}$$

The LSM and LIM designate side and in-plane moments, respectively; i.e., the moments tending to change the yaw angle and nutational frequency, respectively. P indicates pressure, V indicates viscous wall shear, and the final L (lateral) designates sidewall.

The boundary layer assumptions (p. 20 of Reference 7) are retained in the derivation of the shear moment; thus, $\partial\overset{*}{u}/\partial r$, $\partial\overset{*}{u}/\partial\theta$, and $\partial\overset{*}{u}/\partial x$ at $r = 1$ are dropped. For spin-up, additional order of magnitude assumptions are made. While terms of $O(K_0/Re)$ are kept, terms of $O(K_0/Re^{3/2})$ are omitted; thus, U, $\partial U/\partial r$, $\partial W/\partial r$, and $\partial W/\partial z$ are dropped. The term $[V_r(1) - 1]$ appears in the moment coefficient formula, and it is also neglected. Because of the boundary layer in the perturbed flow, it is expected that $|\partial\overset{*}{v}/\partial r|$ and $|\partial\overset{*}{w}/\partial r| \gg [\partial V/\partial r - V/r]$ at $r = 1$ except at very early time when the theory is not applied.

We replace Eq. (5.7) of Reference 7 with the following set of formulas applicable to spin-up for the present circumstances ($\varepsilon = \ell = 0$), where integrands are evaluated at $r = 1$:

$$C_{(LSM)PL} = (2\tau A)^{-1} \quad \text{Real}\left[-i\int_{-A}^{A} x\,(\underline{p}+x)\,dx\right] \tag{3.2a}$$

$$C_{(LIM)PL} = (2\tau A)^{-1} \quad \text{Imag}\left[-i\int_{-A}^{A} x\,(\underline{p}+x)\,dx\right] \tag{3.2b}$$

$$C_{(LSM)VL} = \frac{1}{2\tau A\, Re} \text{ Real } [-i \int_{-A}^{A} \{\frac{\partial \underline{w}}{\partial r} - i\, x \frac{\partial \underline{v}}{\partial r} - i\, x^2 (\frac{\partial V}{\partial r} - \tau)\}\, dx] \tag{3.2c}$$

$$C_{(LIM)VL} = \frac{1}{2\tau A\, Re} \text{ Imag } [-i \int_{-A}^{A} \{\frac{\partial \underline{w}}{\partial r} - i\, x \frac{\partial \underline{v}}{\partial r} - i\, x^2 (\frac{\partial V}{\partial r} - \tau)\}\, dx]. \tag{3.2d}$$

The $\partial V/\partial r$ term replaces unity in Eq. (5.7c) of Reference 7 as a consequence of the sidewall condition on $\overset{*}{v}$ (Eq. (2.6b) in Reference 3). (The third term of the integral in Eqs. (3.2c) and (3.2d) has been retained here and in Reference 7 even through other terms of the same order in Re have been dropped in the boundary layer approximation.) The variables $\underline{p}$, $\underline{v}$, and $\underline{w}$ are evaluated by the formulas in Eq. (2.6). Detailed expressions for the integrals in Eqs. (3.2a) and (3.2b) are given in Eqs. (3.8), (3,9), and (3.10) of Reference 3.

B. Endwall Moment.

$M_{L\tilde{Z}E}$ is the moment about the (transverse) $\tilde{z}$ -axis exerted by the liquid on the endwalls of the container. We restate Eq. (5.12) of Reference 7:

$$M_{L\tilde{Z}E}/(2\pi\rho a^4 \dot{\phi}^2 \tau K_1) = C_{(LSM)PE} \sin \tau\dot{\phi}t + C_{(LIM)PE} \cos \tau\dot{\phi}t + C_{(LSM)VE} \sin \tau\dot{\phi}t + C_{(LIM)VE} \cos \tau\dot{\phi}t. \tag{3.3}$$

The endwall pressure moment coefficients are given by

$$C_{(LSM)PE} = [1/(\tau A)] \text{ Real } [i \int_0^1 r^2 \{\underline{p}(r,A) + A V^2/r\}\, dr] \tag{3.4a}$$

$$C_{(LIM)PE} = [1/(\tau A)] \text{ Imag } [i \int_0^1 r^2 \{\underline{p}(r,A) + A V^2/r\}\, dr], \tag{3.4b}$$

which are the same as those obtained from Eqs. (3.12) - (3.18) in Reference 3.

For the endwall shear

$$C_{(LSM)VE} = - [1/(\tau\, Re)]\ \text{Real}\ \left[\int_0^1 r\ \{\partial\ (\underline{v} - i\ \underline{u})/\partial x\}_{x\,=\,A}\ dr\right] \quad (3.5a)$$

$$C_{(LIM)VE} = - [1/(\tau\, Re)]\ \text{Imag}\ \left[\int_0^1 r\ \{\partial\ (\underline{v} - i\underline{u})/\partial x\}_{x\,=\,A}\ dr\right], \quad (3.5b)$$

the same as Eqs. (5.13c) and (5.13d) of Reference 7. The treatment of the term $\partial\ (\underline{v} - i\underline{u})/\partial x$ parallels that in Section V of Reference 7, where it is shown that the second term dominates the right-hand side of Eq. (5.19). Analogously, here

$$\int_0^1 r\ \{\partial\ (\underline{v} - i\underline{u})/\partial x\}_{x=A}\ dr \approx \beta_E \int_0^1 r\ [-A\{1-2\tau + V_r(r)\} + i\ \Gamma_v(r)]\ dr, \quad (3.6)$$

where

$$\Gamma_v = (\hat{v}_o - i\hat{u}_o)\ A + \sum_{k\,=\,1}^{KF} (\hat{v}_k - i\hat{u}_k)\ \sin\ \lambda_k A + \sum_{j\,=\,1}^{NJ} d_j(\bar{v}_j - i\bar{u}_j)\ \sin\ \mu_j\ A. \quad (3.7)$$

C. Total Moment Coefficient.

The total side moment coefficients due to pressure and shear stress, respectively, are

$$C_{(LSM)P} = C_{(LSM)PL} + C_{(LSM)PE} \quad (3.8a)$$

$$C_{(LSM)V} = C_{(LSM)VL} + C_{(LSM)VE}. \quad (3.8b)$$

The total side moment coefficient is

$$C_{(LSM)} = C_{LSM)P} + C_{(LSM)V}. \quad (3.9)$$

We now define the following side moment coefficient:

$$C_L \equiv C_{LSM}\,\tau. \tag{3.10}$$

For given cylinder, liquid, and spin, C_L is proportional to side moment, regardless of the perturbing frequency.

IV. COMPUTATIONS

A. Results.

We present side moment coefficient histories for the same four combinations of Re and A that were considered in Reference 3. These cover a Reynolds number range of approximately 5×10^3 to 2×10^6. Here we plot C_L instead of C_{LSM}. There is an advantage to this representation in that relative amplitudes of moment are immediately apparent for all perturbing frequencies. Again, the results are compared with inviscid perturbation calculations produced by the method of Murphy.[4]

In Figure 2, C_L histories are shown for five nutational frequencies: τ = 0.04, 0.05, 0.09, 0.12, and 0.14. These were computed with the Wedemeyer laminar Ekman layer spin-up flow model.[8] The results are qualitatively similar to those of Figure 2 in Reference 3. The τ = 0.04 curve asymptotically approaches its maximum with increasing ϕt, indicating a resonance for spun-up liquid. All the other curves have peaks demonstrating resonance with the (k, n) = (3,1) natural oscillation mode of the liquid.* The τ = 0.12 and 0.14 curves have additional peaks (right-hand peaks) produced by resonance with the (k, n) = (5,2) mode. There appears to be a maximum overturning moment that the casing can experience, produced by a particular nutational frequency at a particular time. In this instance the maximizing frequency is very likely close to τ = 0.09 and the time close to ϕt = 1200. For τ = 0.12, the amplitude of the (k, n) = (5,2) mode is small compared to that of the (k, n) = (3,1) mode; however, for τ = 0.14 the two amplitudes are comparable.

The inviscid perturbation results are also shown for τ = 0.04, 0.05, and 0.09; for τ = 0.12 and 0.14 inviscid results are unobtainable because of the presence of the "critical layer" (discussed in References 10 and 11), occurring when $V/r = \tau$ at some r. The relative positions of the curves are

---

*The reader is referred to References 9 and 10 for descriptions of the oscillation modes of a liquid cylinder.

10. B. Vaitekunas and N. Gerber, "Oscillations of a Liquid in a Rotating Cylinder: Part II. Spin-Up," Ballistic Research Laboratory, Aberdeen Proving Ground, Maryland, ARBRL-TR-02489, May 1983. (AD A130041)

11. B. Vaitekunas and N. Gerber, "A Study of the Critical Layer in a Rotating Liquid Payload," Ballistic Research Laboratory, Aberdeen Proving Ground, Maryland, ARBRL-TR-02582, August 1984. (See also AIAA Paper No. 84-0348, January 1984.)

similar to those in Figure 2 of Reference 3, but the relative discrepancies are now larger, for a discrepancy in viscous shear moment is now added to that in pressure moment. However, the predictions of times of peak moments still agree to within about 0.07 s.

Figure 3 deals with a case of smaller spin-up time (spin-up time defined in Chapter I of Reference 12); therefore, the interval of interest applies to smaller $\dot{\phi}t$. The Ekman layer is taken to be laminar in the spin-up flow model. In Figure 4 the eigenfrequency histories of five oscillation modes during spin-up show the times when resonances with the coning frequency τ = 0.15 occur, i.e., when C_R = 0.15. The time of occurrence of the peak obtained by the present method, $\dot{\phi}t \approx 225$, indicates a resonance with the (k, n) = (3,1) mode. The inviscid perturbation method fails to show this resonance; possibly the method deteriorates with decreasing time shortly before it breaks down due to the critical layer. The inviscid computation shows a prominent peak at $\dot{\phi}t \sim 250$ in Figure 3 where the frequencies (computed with inviscid perturbations) of the (k, n) = (5,2) and (7,3) modes are approximately equal to 0.15. The present calculation shows no indication of resonance at this time, though a jog appears in $C_{(LSM)P}$ in Figure 3 of Reference 3.*

The present computation does not extend below $\dot{\phi}t \approx 200$ because of problems (described in Chapter II.C of Reference 3) which arise at "small" times. These are manifested in the difficulty encountered in obtaining certain of the μ_j's. While this difficulty is not necessarily insuperable, the required labor can at times render the effort infeasible.

In Figure 5, moment coefficient histories are shown for Re = 1.85×10^6 for two aspect ratios differing by 2.55%. The turbulent Ekman layer was employed in the spin-up model here. The sensitivity of side moment to c/a is borne out by the two widely differing responses to disturbances of the same frequency. Both cases can be plotted on the same graph since the times of significant variation in the two sets of curves differ markedly ($\dot{\phi}t \sim$ 10,000 for A = 4.973 and $\dot{\phi}t \sim$ 40,000 for A = 5.100).

We first consider the c/a = 5.100 case. Figure 4 in Reference 3 demonstrates the agreement between the present and inviscid perturbation methods for the pressure contribution alone. Discrepancies between the two outputs are noticeably increased when shear moment is included, particularly near the times of occurrence of the peaks. In the present method, the viscous shear increases the overturning moment by as much as 25% at $\dot{\phi}t$ = 42,000; whereas, the inviscid perturbation method generally yields a slight decrease. However, the two curves approach each other as $\dot{\phi}t$ increases, reaching a limiting value

---

*[illegible] of Reference 3 is incorrect in the region of $\dot{\phi}t$ = [illegible] the oscillate exhibits no peak there.

12. [illegible], "Viscous Effects in the Wedemeyer Model of Spin-Up [illegible]," Ballistic Research Laboratory, Aberdeen Proving Ground, Maryland, [illegible], June [illegible]. (AD [illegible])

of $C_L = 2.95 \times 10^{-4}$. The predictions of times of peak moments differ between the two methods by approximately 1.6 s for $C_{L_{SM}}$ (Figure 4 of Reference 3) and by approximately 1.8 s for C_L.

For c/a = 4.973 the addition of shear moment does not affect the inviscid output qualitatively, as indicated by inspection of present Figure 5 and Figure 5 of Reference 3. However, it drastically changes the picture for the present method; the C_L curve has a minimum with negative value as before, but it also has a peak immediately afterward. The peaks for both aspect ratios indicate resonance with the (k, n) = (5,1) mode of the liquid.

B. Accuracy of Results.

Confidence in the numerical results requires some estimate of their accuracy. A thorough-going error study for wide ranges of physical parameters is not feasible; we confine our attention to the cases treated in Section IV.A. There are at least twelve parameters in the spin-up and perturbed Navier-Stokes calculations alone that control the accuracy of the numerical procedures. Accuracy as used here is quite different from validation of the theory. There are, in fact, no experimental data to compare with the present theory.

In all cases we computed spin-up profiles with r-interval $\Delta r = 1/200$ and time interval $\Delta (\dot{\ddagger} t)$ small enough so that five or fewer iterations were required for convergence. For the perturbation equations, we took $\Delta r = 1/1000$ and performed no less than fifty orthonormalizations. We used as many as thirty terms of the power series to evaluate the solution to the perturbation equations at r = 0.001 where the numerical integration began, and we used seven terms ($b_k \sin \lambda_k x$) in the biorthogonal expansion of the function x. In all iterative processes, we required convergence at least to five decimal places.

In this problem an additional factor, apart from those introduced by the numerical operations, must be considered; namely, the error Er of Eq. (2.19) resulting from approximating $\psi(r)$ by a finite series, $\sum_{j=1} e_j w_j(r)$, in Eqs. (2.16) and (2.17). This approximation is made in order to minimize the overall error resulting from failure of the solution to satisfy the endwall boundary condition identically. In the procedure of Reference 3, designated "Method I" here, we used NJ $\bar{w}_j$'s; whereas, in the present procedure, designated "Method II," we employ (NJ + 2) $\bar{w}_j$'s, the first NJ of which are identical to those of Method I. Whenever possible, we set NJ = 6, but it is not always possible to do so.

Figures 6, 7, 8 and 9 present comparisons of errors for Methods I and II. In both methods, $\psi(r) \equiv 0$ and all e_j's = 0 at solid body rotation, so that in principle Er ($\dot{\ddagger} t = 0$) is indeterminate. Results indicate a general trend in which the error decreases as time decreases from $\dot{\ddagger} t = 0$, reaches a minimum, and

then increases, sometimes at a rapid rate, as $t \to 0$. In Figure 6, Method II yields a considerably smaller error than Method I, being always less than 1/2 percent; the same result holds for $\tau = 0.04$ and 0.09. One would expect a more accurate approximation from Method II because there are NJ + 2, as compared to NJ, functions with which to approximate $\psi(r)$. This is true in most of our cases. However, the error of Method II can also become very large, as shown in Figure 7. We note that $\psi(r)$ and the functions with which it is fitted generally have sharp dips or spikes near r = 1 because of the sidewall boundary layer. Furthermore, at early time when a critical layer is present, these functions often have sharp oscillations in the critical layer. These two factors should account in part for the large error of Method II at early time.

Method II produces a considerably smaller error than Method I for the case in Figure 8 and for the c/a = 5.100 case in Figure 9. For the c/a = 4.973 case in Figure 9 the region of resonance is at early time, and the two methods have comparable errors. In all the error plots except those in Figure 7, six eigenvalues μ_j and corresponding eigenfunctions were used. In the plot for $\tau = 0.12$, due to the difficulty of computing other eigenvalues, only the n = 1,2,3,4 modes were used for $\dot{\phi}t \geq 1000$ and the n = 1,2,4 modes for $\dot{\phi}t < 1000$.

The eigenvalues μ, together with their associated eigenfunctions, $\bar{w}(r)$, are important parameters of the solution, not only in the number used but also in the choice of eigenvalues and functions when a choice is available. At solid body rotation the radial oscillation modes are identified according to the increasing value of the real part of the eigenvalue and designated as n = 1,2, etc. The oscillation modes retain their identity with decreasing time, but eventually their history has to be traced in small time decrements since some of the Real (μ_n) vs t curves cross.

Experience indicates that the most accurate calculations are obtained when the lowest possible modes are employed in the approximation to $\psi(r)$; e.g., if NJ = 4, the j = 1, 2, 3, 4 in Eq. (2.6) should correspond to n = 1, 2, 3, 4. Table I provides an illustration. To three figures, the (n = 1, 2, 3, 4) combination gives the same C_L values as the six-mode calculation, which presumably is the most accurate choice; and the C_L from the (n = 1, 2, 3) combination differs from these by less than 3%. It should be noted, however, that agreement between the four- and six-mode approximations is not always as good as that obtained in this particular case. The other combinations give values of C_L that differ by at least 10 and 18% from 0.0204. In this instance the sensitivity to choice of modes is more notable than sensitivity to number of modes. The third and fourth combinations in Table 1 can arise in the actual moment calculation. Under certain circumstances, the iteration process may converge to an eigenvalue other than the one being sought if the initial guess is not sufficiently close to the final answer. This phenomenon is discussed on page 21 of Reference 3. In the case shown in Table 2, the two determinations of C_L differ by about 3 .

Figures 10, 11, and 12 compare the C_L's obtained by Methods I and II. For the Re = 39,772 and Re = $1.85 \cdot 10^6$ cases there is general agreement between the outputs of the two methods even though the τ's disagree (Figures 6 and 9). Thus, τ is not a sensitive indicator of the effect on C_L of the

method employed. For the Re = 4974 case, the discrepancies are appreciable; e.g., at $\dot{\phi}t$ = 400 the C_L of Method I is less than half of the C_L of Method II. In light of the errors plotted in Figure 8, we conclude that Method II yields the more accurate value of C_L in this particular case.

TABLE 1. EFFECT OF RADIAL MODES ON ERROR AND MOMENT COEFFICIENT: Re = 4974, A = 3.30, τ = 0.15, $\dot{\phi}t$ = 220.

Mode (n) Combinations	Er	C_L
1, 2, 3, 4, 5, 6	0.14	0.02044
1, 2, 3, 4	0.58	0.02043
1, 3, 4, 5	3.65	0.02268
2, 3, 4, 6	10.89	0.01674
1, 2, 3	1.38	0.02051

TABLE 2. Er AND C_L FOR TWO SETS OF MODES: Re = 39,772, A = 3.12, τ = 0.14, $\dot{\phi}t$ = 1000.

Mode (n) Combinations	Er	C_L
1, 2, 3, 4, 5, 6	0.97	0.000637
1, 2, 3, 4	4.14	0.000585

V. SUMMARY

The primary mechanism for producing unstable motion of projectiles with fully spun-up liquid payload is resonance between the coning motion of the projectile and inertial oscillations of the contained liquid. Resonance also occurs early in the flight during spin-up, but the transient natures of the fluid flow and projectile angular motion make prediction of instability more difficult than for solid body rotation. This report describes a procedure, based on linearized flow, for calculating the side moment exerted by the liquid on the casing during spin-up for the special case of constant coning frequency and zero yaw growth. Here the moment due to shear forces is included in addition to that due to pressure forces. The heuristic approach of Murphy[4] is used which makes crucial assumptions regarding time-dependence

of the flow and the endwall boundary condition. Because of the specialized angular motion the present treatment cannot simulate actual flight, although it can simulate performable gyroscope experiments. The validity of this method is expected to be strongest at late time and diminish with decreasing time.

Calculations were performed for four combinations of Re and A and a variety of nutational frequencies. The peaks of the C_L vs $\dot{\phi}t$ curves indicate transient coincidence of certain inertial frequencies of the liquid with the frequency of coning. For a given container, payload, and spin, there is a finite frequency which maximizes the side moment during the course of spin-up. The duration of a side moment surge, as well as its amplitude, will undoubtedly be a factor in determining onset of instability in a free-flight situation. Comparison of output with results of the inviscid perturbation method shows qualitative agreement at late time but differing indications of resonance at early time, as, for example, in Figure 3.

In the current analysis an ad hoc correction was made to the endwall boundary condition which is an extension of the correction for the solid body rotation problem. A subsequent refinement should be the inclusion of the Ekman layers in the basic flow. This step is necessary in order to have a rational approximation to the solution. It is not expected to be easy to achieve.

ACKNOWLEDGEMENTS

The author is pleased to acknowledge the help of Ms. Joan M. Bartos, who programmed and performed the moment calculations. Appreciation is extended to Dr. Raymond Sedney for his overall guidance. The moment data for inviscid perturbation were obtained from calculations performed with a program prepared by Mr. James W. Bradley.

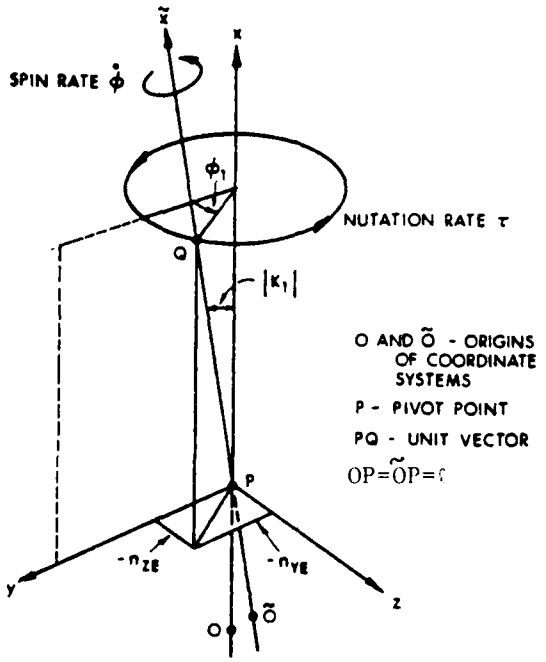

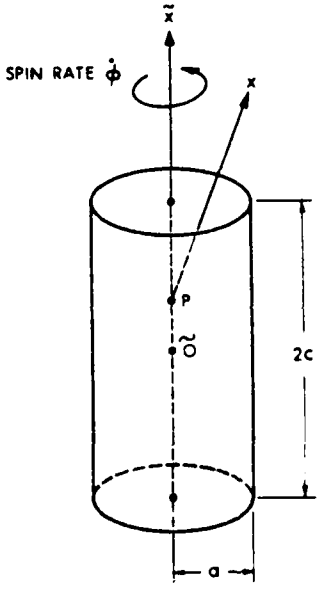

Figure 1. Diagrams of Coordinates and Cylinder.

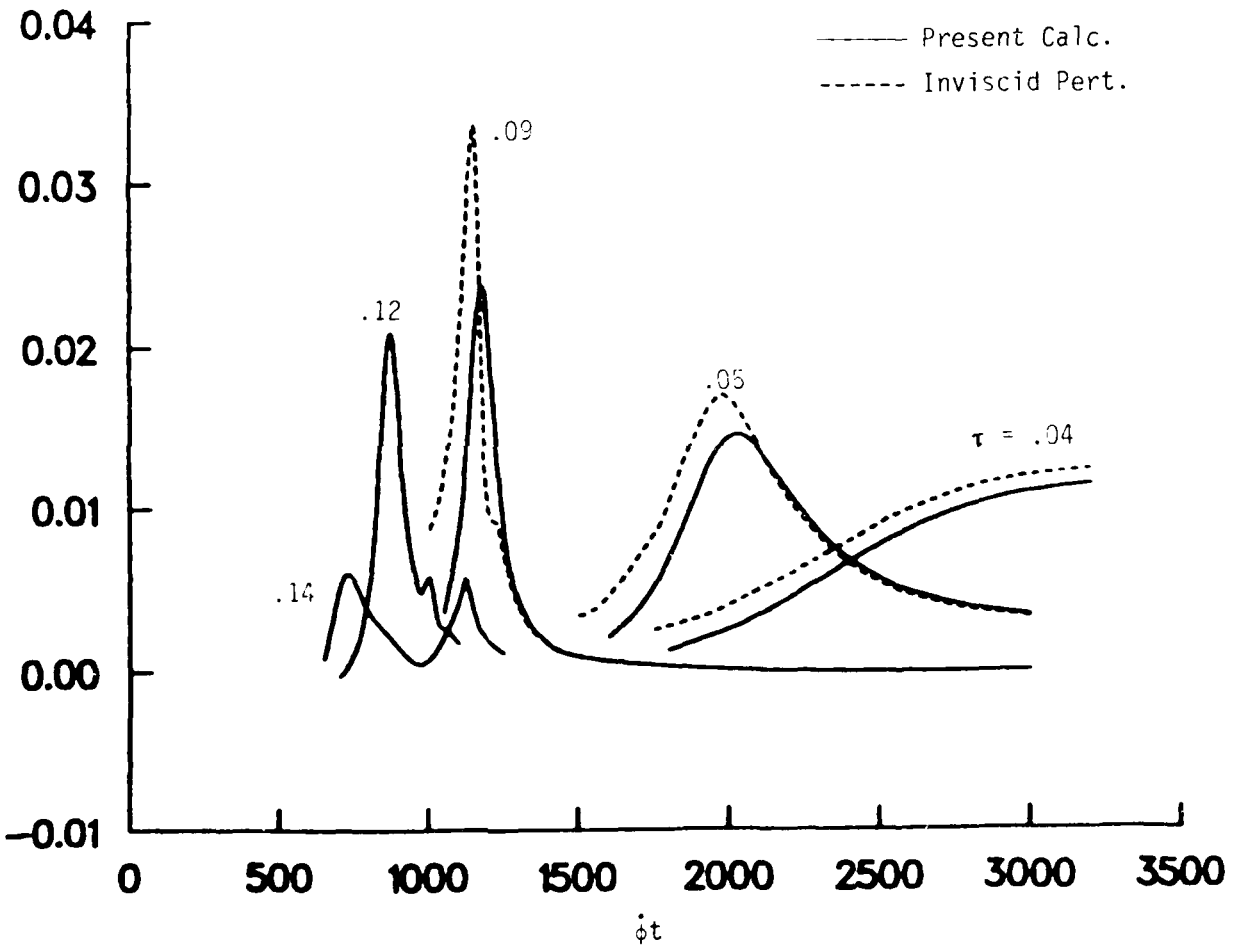

Figure 2. Side Moment Coefficient Histories for Five Nutational Frequencies, Re = 39772, A = 3.12, $\dot{\phi}$ = 754 rad/s.

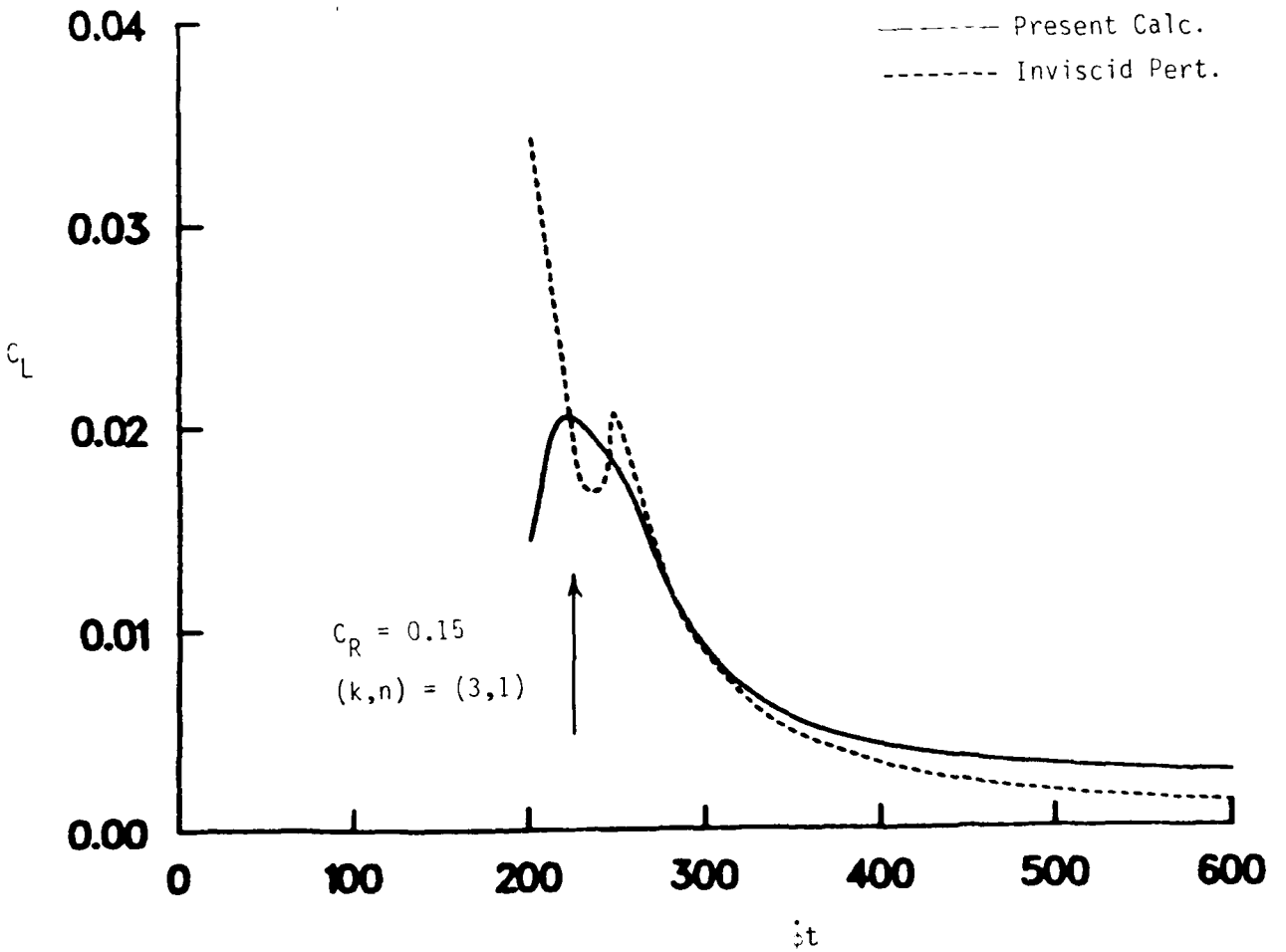

Figure 3. Side Moment Coefficient History, Re = 4974, A = 3.30, $\dot{\gamma}$ = 8937 rad/s, τ = 0.15.

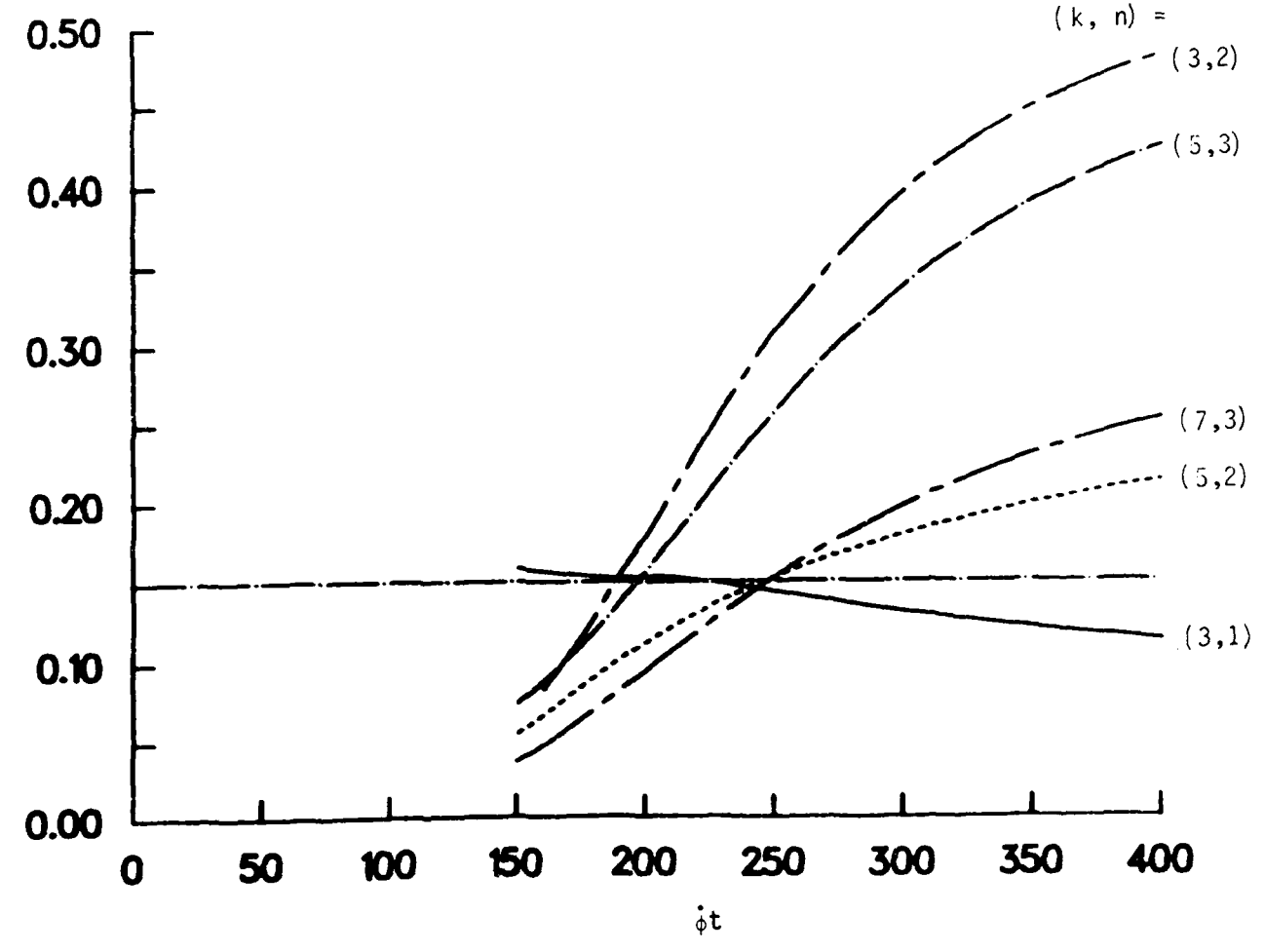

Figure 4. Spin-Up Eigenfrequency Histories for Five Modes, Re = 4974, A = 3.30.

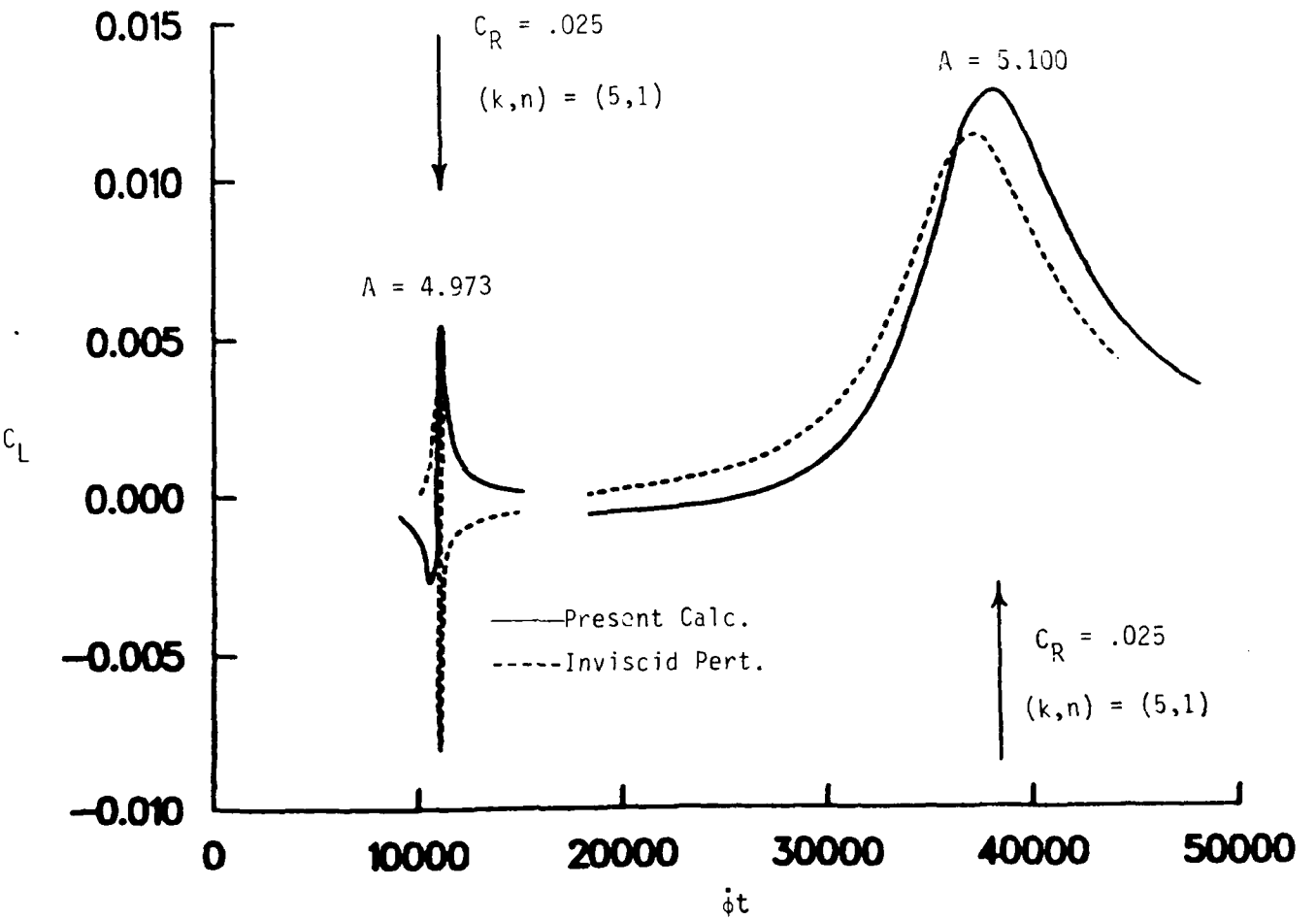

Figure 5. Side Moment Coefficient Histories for Two Aspect Ratios, Re = 1.85×10^6, $\dot{\phi}$=641 rad/s, τ = 0.025.

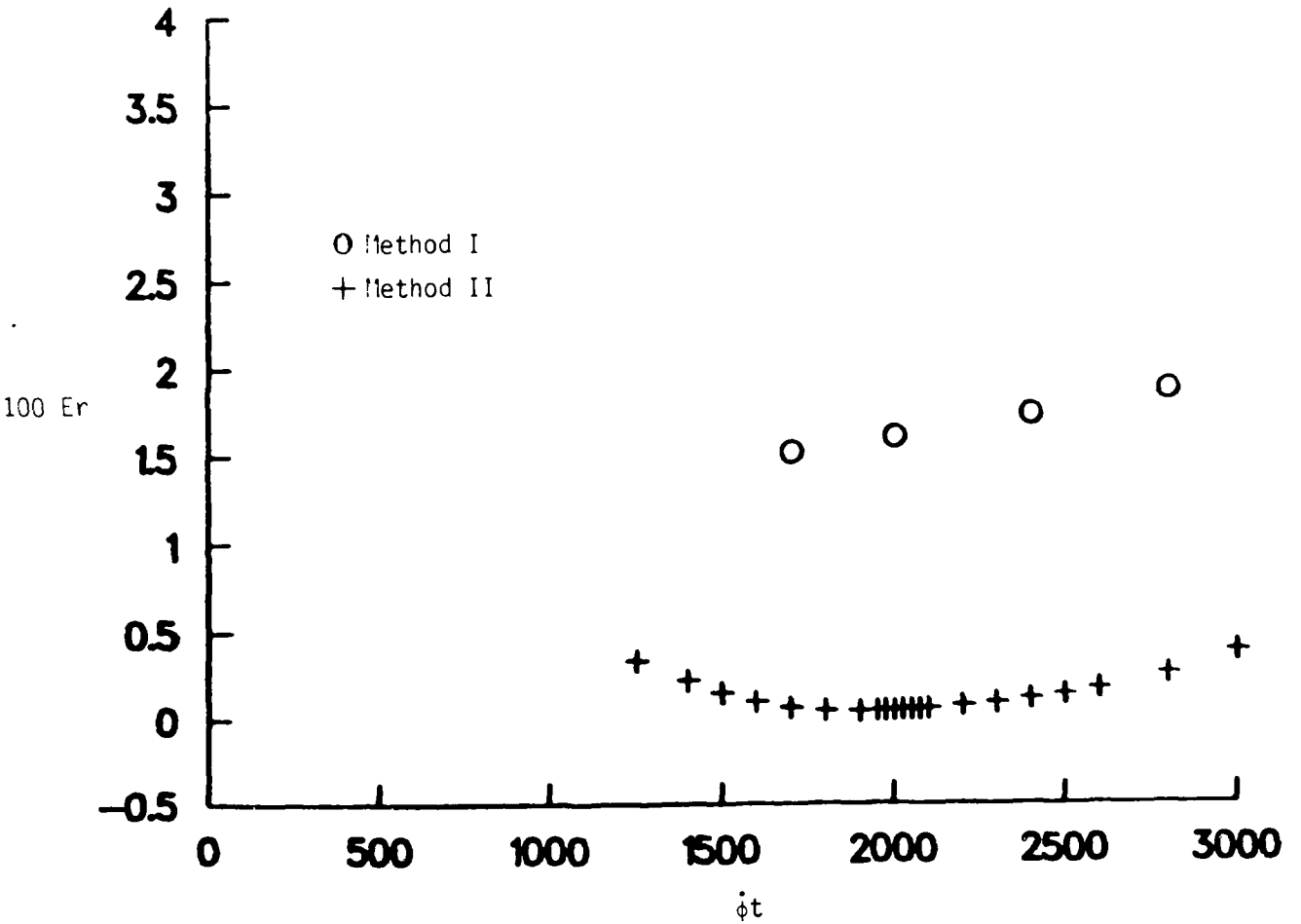

Figure 6. Comparison Between Percentage Errors of Methods I and II, Re = 39772, A = 3.12, τ = 0.05.

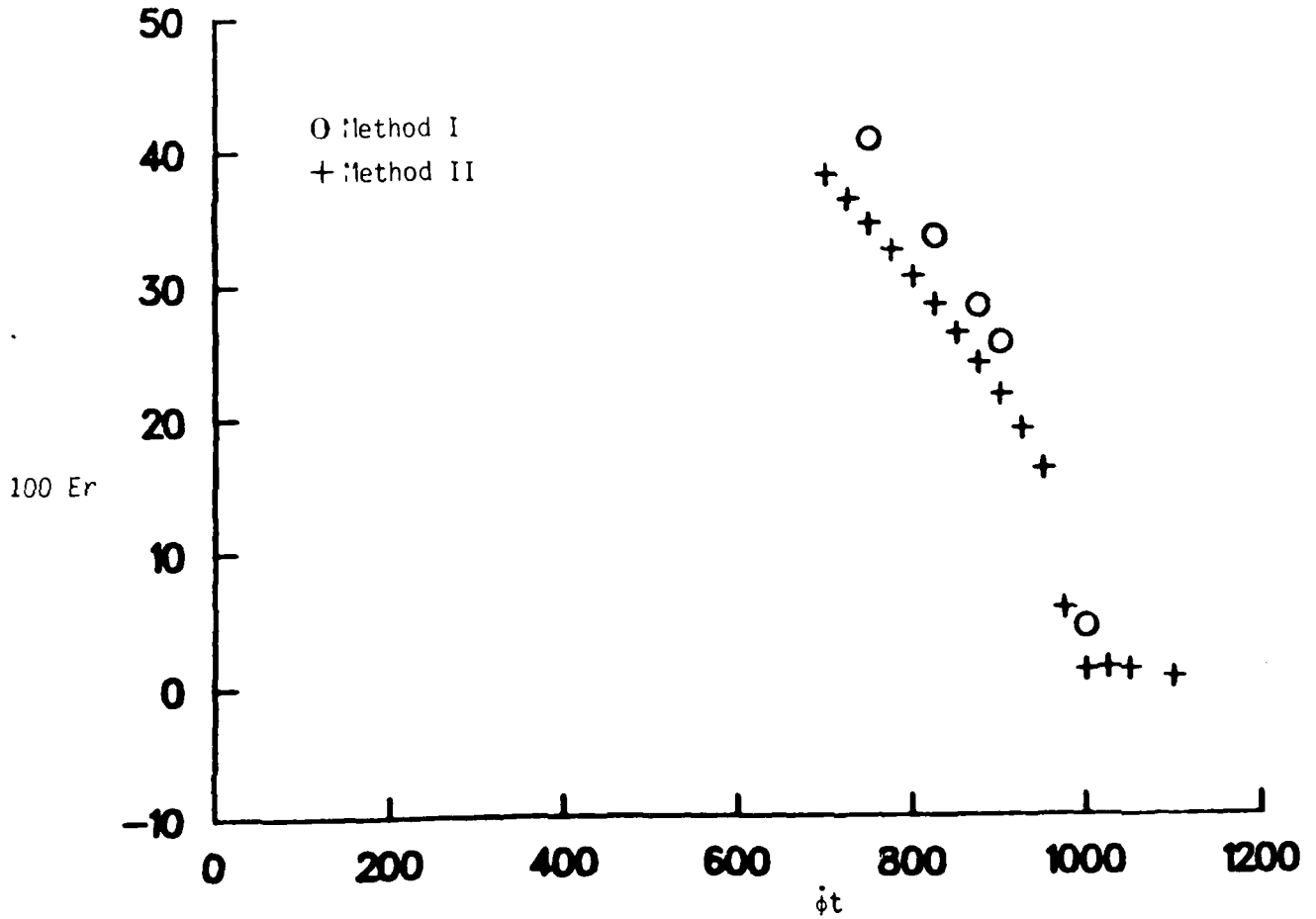

Figure 7. Comparison Between Percentage Errors of Methods I and II, Re = 39772, A = 3.12, τ = 0.12.

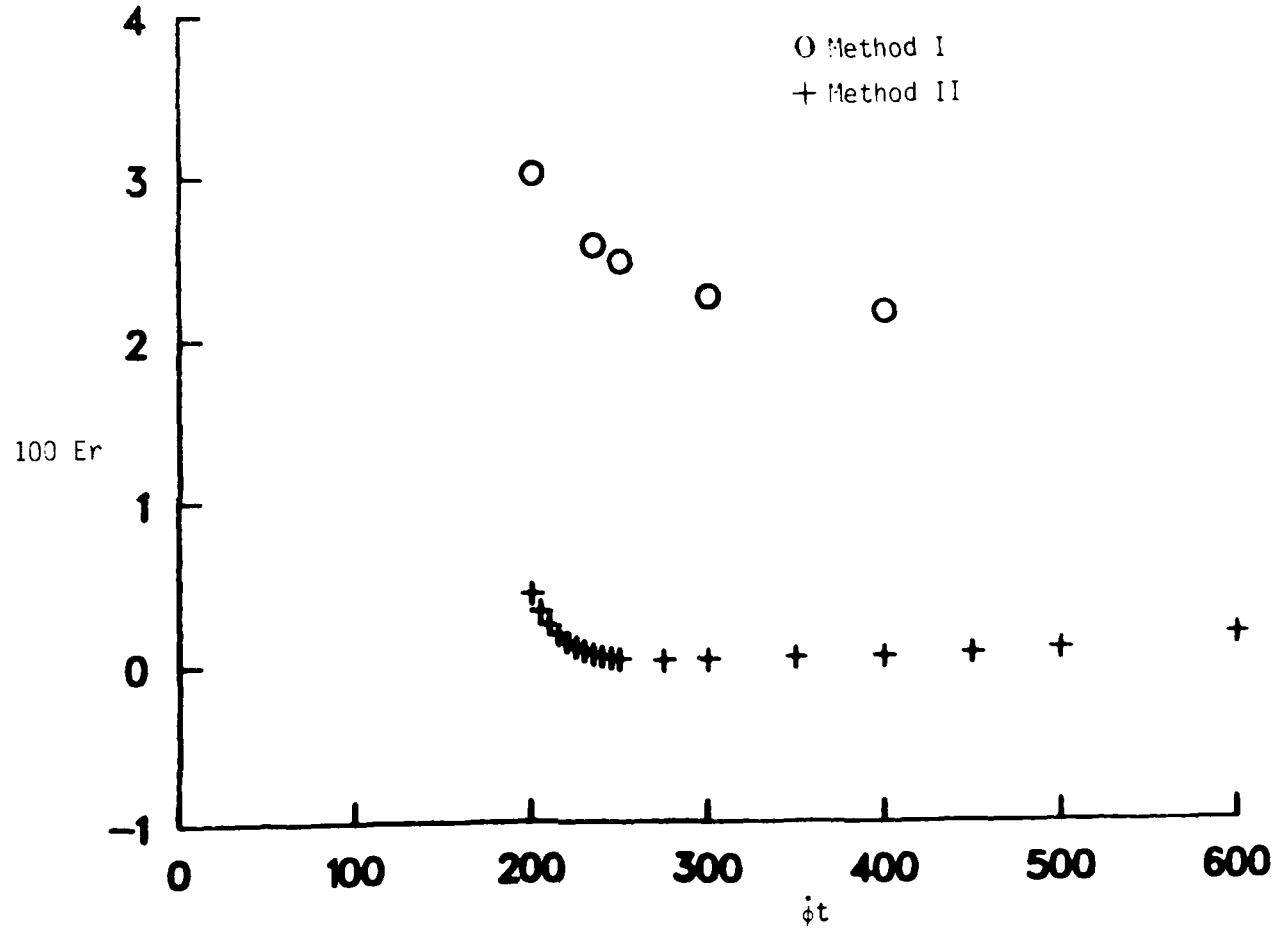

Figure 8. Comparison Between Percentage Errors of Methods I and II, Re = 4974, A = 3.30, τ = 0.15.

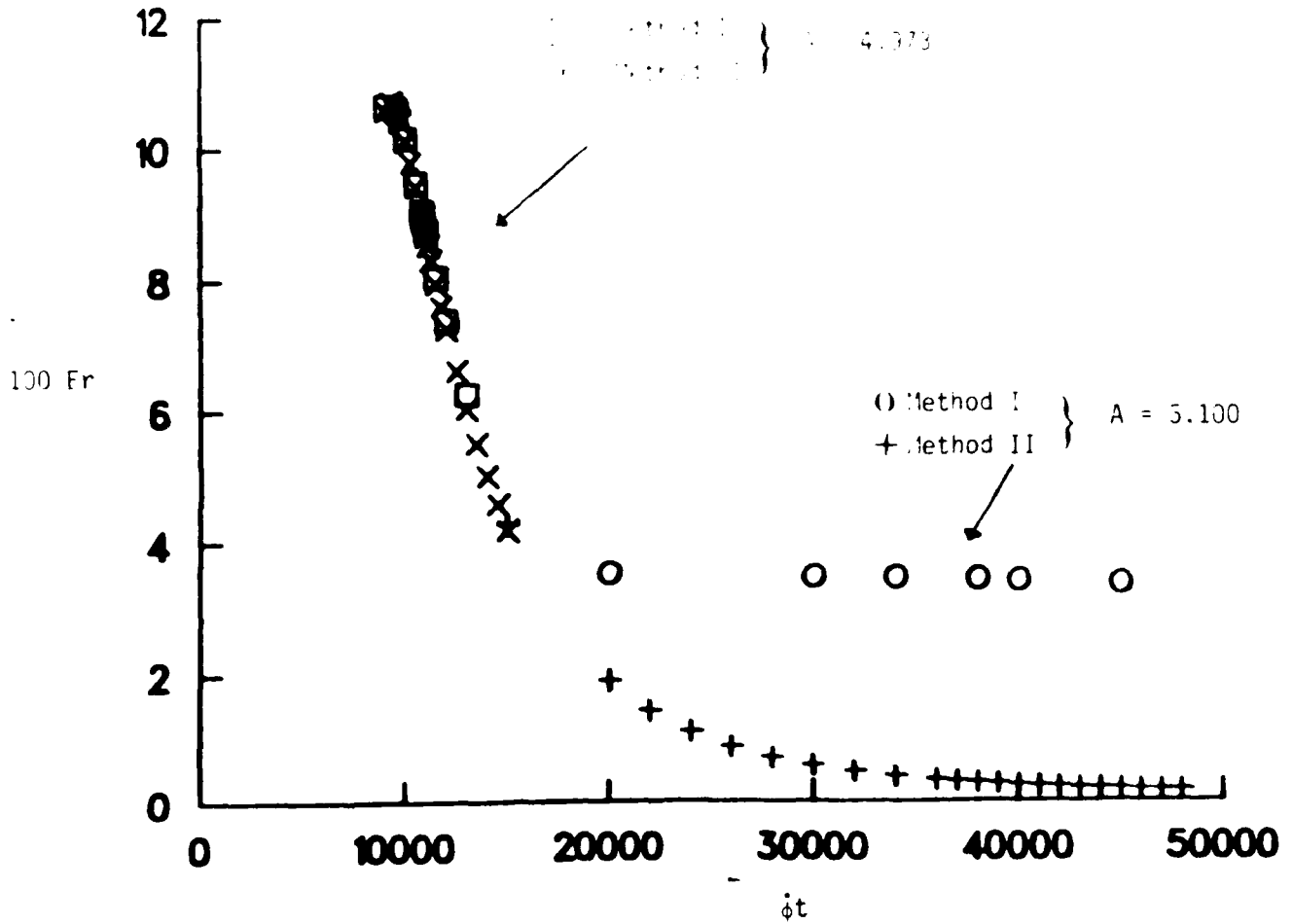

Figure 9. Comparison Between Percentage Errors of Methods I and II, $Re = 1.85 \times 10^6$, $\tau = 0.025$.

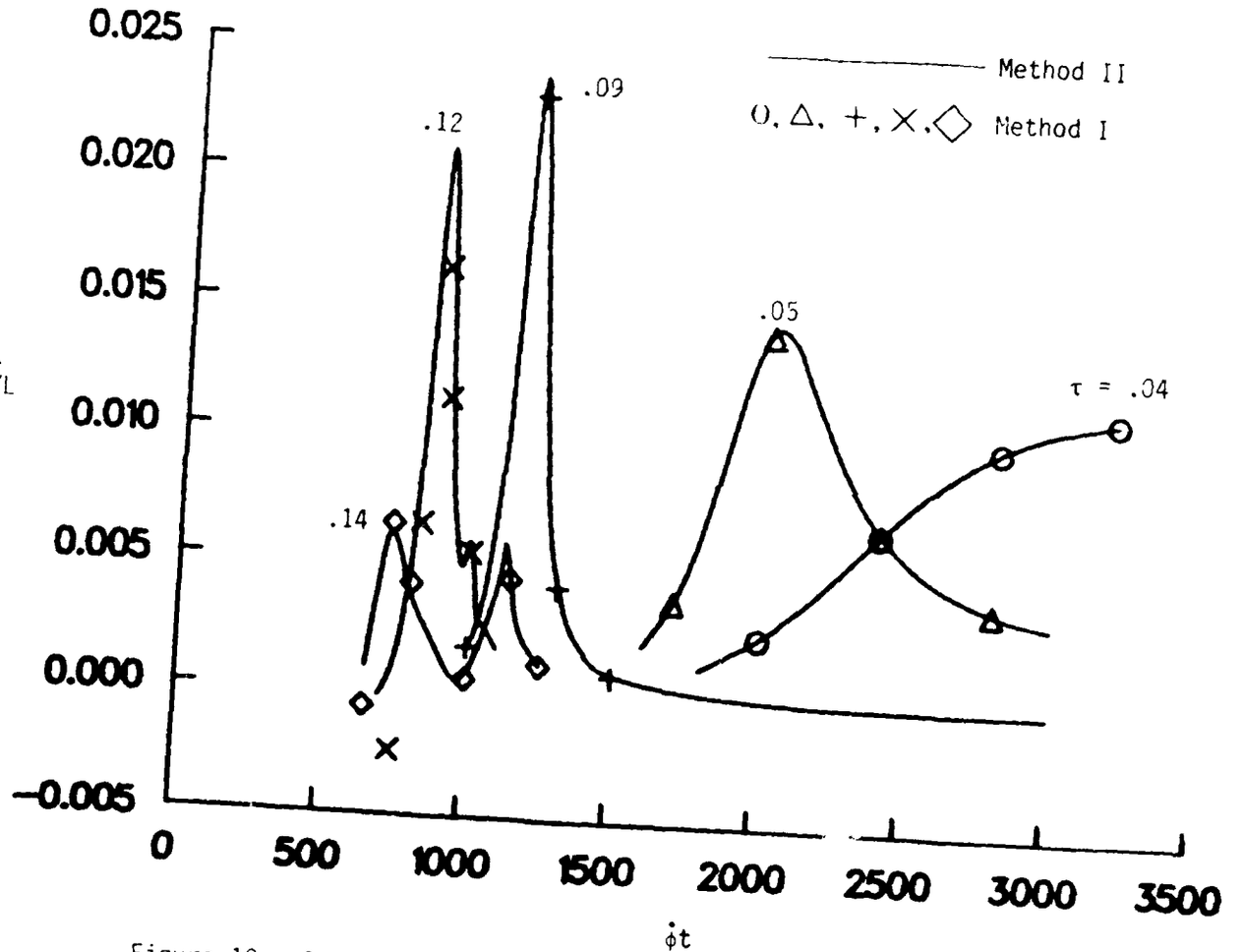

Figure 10. Comparison Between Side Moment Coefficients of Methods I and II, Re = 39772, A = 3.12.

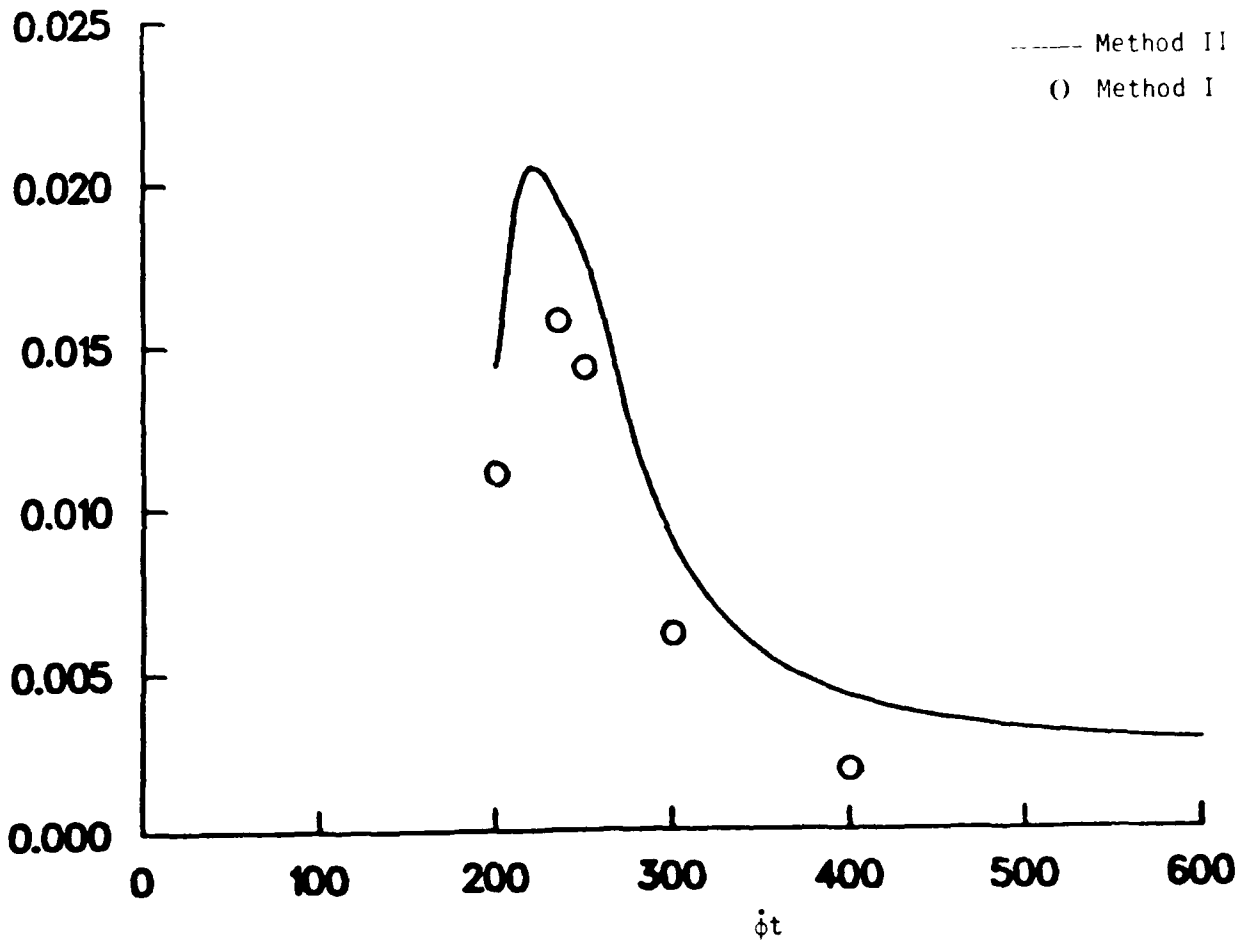

Figure 11. Comparison Between Side Moment Coefficients of Methods I and II, Re = 4974, A = 3.30, τ = 0.15.

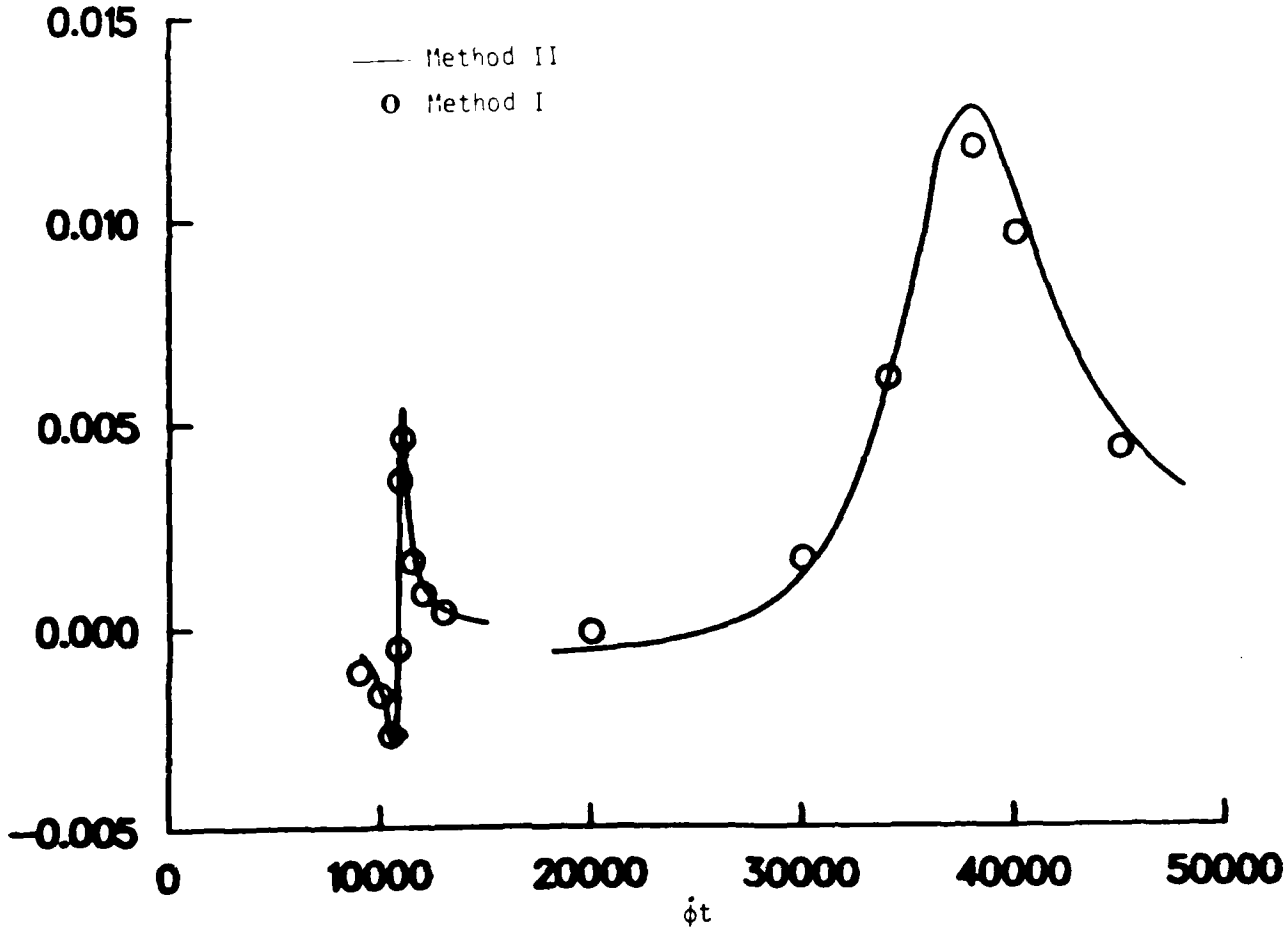

Figure 12. Comparison Between Side Moment Coefficients of Methods I and II, Re = 1.85×10^6, $\tau = 0.025$.

REFERENCES

1. K. Stewartson, "On the Stability of a Spinning Top Containing Liquid," Journal of Fluid Mechanics, Vol. 5, Part 4, 1959.

2. E. H. Wedemeyer, "Viscous Corrections to Stewartson's Stability Criterion," Ballistic Research Laboratory, Aberdeen Proving Ground, Maryland, BRL Report No. 1287, June 1966. (AD 489687)

3. N. Gerber, "Contribution of Pressure to the Moment During Spin-Up on a Nutating Liquid-Filled Cylinder: Ad Hoc Model," Ballistic Research Laboratory, Aberdeen Proving Ground, Maryland, ARBRL-TR-02563, June 1984. (AD A143678)

4. C. H. Murphy, "Moment Induced by Liquid Payload During Spin-Up Without a Critical Layer," Ballistic Research Laboratory, Aberdeen Proving Ground, Maryland, ARBRL-TR-02581, August 1984. (AD A145716). (See also AIAA 22nd Aerospace Sciences Meeting, Reno, Nevada, AIAA Paper No. 84-0229, January 1984.)

5. C. H. Murphy, "Angular Motion of a Spinning Projectile with a Viscous Liquid Payload," Ballistic Research Laboratory, Aberdeen Proving Ground, Maryland, ARBRL-MR-03194, August 1982. (AD A118676) (See also Journal of Guidance, Control, and Dynamics, Vol. 6, July-August 1983, pp. 280-286.)

6. N. Gerber, R. Sedney, and J. M. Bartos, "Pressure Moment on a Liquid-Filled Projectile: Solid Body Rotation," Ballistic Research Laboratory, Aberdeen Proving Ground, Maryland, ARBRL-TR-02422, October 1982. (AD A120567)

7. N. Gerber and R. Sedney, "Moment on a Liquid-Filled Spinning and Nutating Projectile: Solid Body Rotation," Ballistic Research Laboratory, Aberdeen Proving Ground, Maryland, ARBRL-TR-02470, February 1983. (AD A125332)

8. E. H. Wedemeyer, "The Unsteady Flow Within a Spinning Cylinder," Ballistic Research Laboratory, Aberdeen Proving Ground, Maryland, BRL Report No. 1225, October 1963. (AD A431846) (See also Journal of Fluid Mechanics, Vol. 20, Part 3, 1964, pp. 383-399.)

9. C. W. Kitchens, Jr., N. Gerber, and R. Sedney, "Oscillations of a Liquid in a Rotating Cylinder: Part I. Solid-Body Rotation," Ballistic Research Laboratory, Aberdeen Proving Ground, Maryland, ARBRL-TR-02081, June 1978. (AD A057759)

10. R. Sedney and N. Gerber, "Oscillations of a Liquid in a Rotating Cylinder: Part II. Spin-Up," Ballistic Research Laboratory, Aberdeen Proving Ground, Maryland, ARBRL-TR-02489, May 1983. (AD A129094)

11. R. Sedney and N. Gerber, "A Study of the Critical Layer in a Rotating Liquid Payload," Ballistic Research Laboratory, Aberdeen Proving Ground, Maryland, ARBRL-TR-02582, August 1984. (See also AIAA Paper No. 84-0342, January 1984.)

12. R. Sedney and N. Gerber, "Viscous Effects in the Wedemeyer Model of Spin-Up from Rest," Ballistic Research Laboratory, Aberdeen Proving Ground, Maryland, ARBRL-TR-02493, June 1983. (AD A129506)

APPENDIX A

CALCULATION OF e_j's

APPENDIX A. CALCULATION OF e_j's

Eq. (2.16) is restated:

$$R(r) = \psi(r) - \sum_{j=1}^{NJ+2} e_j \bar{w}_j(r). \qquad (A.1)$$

We now define the following elements:

$$s_n = \int_0^1 \psi(r) \cdot \text{conj}\,[\bar{w}_n(r)]\, dr \qquad n = 1,\ldots,NJ+2 \qquad (A.2)$$

$$s_{n,j} = \int_0^1 \bar{w}_j \cdot \text{conj}\,[\bar{w}_n]\, dr \qquad n,j = 1,\ldots,NJ+2, \qquad (A.3)$$

where conj $[\bar{w}_n]$ is the complex conjugate of $\bar{w}_n$.

The e_j's which minimize the error integral γ of Eq. (2.18) are found by solving the following system of linear complex equations:

$$\sum_{j=1}^{NJ+2} s_{nj}\, e_j = s_n \qquad n = 1,\ldots,NJ+2. \qquad (A.4)$$

LIST OF SYMBOLS

a	cross-sectional radius of cylinder, Figure 1 [cm]
A	$= c/a$, aspect ratio of cylinder
b_k	biorthogonal coefficients for series expansion of x in interval $-A \leq x \leq A$, Eq. (2.21)
c	half-height of cylinder [cm]
C_L	$= C_{LSM}\ \tau$, a side moment coefficient
$C_{(LIM)PE}$	endwall pressure in-plane moment coefficient, Eqs. (3.3) and (3.4b)
$C_{(LIM)PL}$	sidewall pressure in-plane moment coefficient, Eqs. (3.1) and (3.2b)
$C_{(LIM)VE}$	endwall viscous shear in-plane moment coefficient, Eqs. (3.3) and (3.5b)
$C_{(LIM)VL}$	sidewall viscous shear in-plane moment coefficient, Eqs. (3.1) and (3.2d)
C_{LSM}	total side moment coefficient, Eq. (3.9)
$C_{(LSM)P}$	pressure side moment coefficient, Eq. (3.8a)
$C_{(LSM)PE}$	endwall pressure side moment coefficient, Eqs. (3.3) and (3.4a)
$C_{(LSM)PL}$	sidewall pressure side moment coefficient, Eqs. (3.1) and (3.2a)
$C_{(LSM)V}$	viscous shear side moment coefficient, Eq. (3.8b)
$C_{(LSM)VE}$	endwall viscous shear side moment coefficient, Eqs. (3.3) and (3.5a)
$C_{(LSM)VL}$	sidewall viscous shear side moment coefficient, Eqs. (3.1) and (3.2c)
C_R	natural oscillation frequency of rotating liquid/

d_j	coefficient in series given by the 3rd terms on right-hand sides of Eqs. (2.6a) - (2.6d)
e_j	coefficient defined in Eq. (2.17a)
Er	relative error measure defined in Eq. (2.19)
f	$\equiv (1 - i\varepsilon)\tau$, complex representation of angular motion, Eq. (1.3)
$g(e_j)$	error integral defined in Eq. (2.18)
k	index of axial eigenfunction and eigenvalue
k_1, k_2, k_3	coefficients of combination of linearly independent solutions, (Eq. (2.12)
KF	index of final term of sin $\lambda_k x$ and cos $\lambda_k x$ in Eq. (2.6)
K_0	yaw amplitude at time t = 0
K_1	$K_0\, e^{\varepsilon\tau\dot{\phi}t}$, yaw amplitude at time t, Eq. (1.3)
ℓ	nondimensional x (and $\tilde{x}$) coordinate of pivot point
$M_{L\tilde{L}}$, $M_{L\tilde{E}}$	sidewall and endwall contributions, respectively, to liquid moment about $\tilde{z}$-axis [g cm^2/s^2]
n	index of radial mode for eigenfrequency, C_R
$n_{y\tilde{E}}$, $n_{z\tilde{E}}$	components in the y, z plane of a unit vector lying on the $\tilde{x}$-axis
N_k	number of terms in the series given by the 3rd terms of the right-hand sides of Eqs. (2.6)

p	pressure/$(\rho a^2 \dot{\phi}^2)$
$\underline{p}\ (r,x)$	r, x variation of perturbation pressure/$(K_0 \rho a^2 \dot{\phi}^2)$
$\bar{p}_j\ (r)$	jth radial eigenfunction in series given by the 3rd term in Eq. (2.6d)
$\hat{p}_0(r)$	first term in solution to $\underline{p}$, Eq. (2.6d)
$\hat{p}_k(r)$	coefficient of sin $\lambda_k x$ in series given by the 2nd term of the right-hand side of Eq. (2.6d)
p^*	perturbation pressure/$(K_0 \rho a^2 \dot{\phi}^2)$, Eq. (2.1d)
P	axisymmetric unperturbed pressure/$(\rho a^2 \dot{\phi}^2)$, Wedemeyer spin-up model, Eq. (2.1d)
r	(1/a) × radial coordinate in inertial coordinate system
$R(r)$	error function defined in Eq. (2.16)
Re	Reynolds number = $a^2 \dot{\phi}/\nu$
Re_E	"effective" Reynolds number, Eq. (2.5)
t	time [s]
u, v, w	$(1/[a\dot{\phi}])$ × radial, azimuthal, axial velocity components, respectively, in inertial frame
$\underline{u}, \underline{v}, \underline{w}$	$(1/[K_0 a \dot{\phi}])$ × r, x variation of perturbation radial, azimuthal, axial velocity components, Eq. (2.2)
$\bar{u}_j, \bar{v}_j, \bar{w}_j$	coefficients of sin $\mu_j x$ and cos $\mu_j x$ in series expansions for $\underline{u}$, $\underline{v}$, $\underline{w}$, $\underline{p}$ (3rd terms of right-hand sides of Eqs. (2.6))

$\hat{u}_k$, $\hat{v}_k$, $\hat{w}_k$	coefficients of sin $\lambda_k x$ and cos $\lambda_k x$ in series expansions for $\underline{u}$, $\underline{v}$, $\underline{w}$ (2nd terms of right-hand sides of Eqs. (2.6))
$\hat{u}_o$, $\hat{v}_o$, $\hat{w}_o$	1st terms in right-hand sides of Eqs. (2.6a), (2.6b), and (2.6c)
$\overset{*}{u}$, $\overset{*}{v}$, $\overset{*}{w}$	$(1/[K_o a \dot{\phi}])$ × radial, azimuthal, axial perturbation velocity components in inertial system, Eqs. (2.1) and (2.2)
U, V, W	$(1/[a\dot{\phi}])$ × radial, azimuthal, axial velocity components of axisymmetric unperturbed flow, Eq. (2.1)
$\hat{U}_i$, $\hat{V}_i$, $\hat{W}_i$	(i = 1, 2, 3) linearly independent solutions which are combined to obtain $\hat{u}_o$, $\hat{v}_o$, $\hat{w}_o$, Eq. (2.12)
x, y, z	rectangular coordinates in inertial system (x-axis along trajectory) [length/a], y = r cos θ, z = r sin θ
$\tilde{x}$, $\tilde{y}$, $\tilde{z}$	rectangular coordinates in aeroballistic system ($\tilde{x}$-axis along cylinder axis) [length/a]
β_E	quantity defined in Eq. (2.4b), used in evaluating $C_{(LSM)VE}$
δc_E	correction term in ad hoc endwall boundary condition, Eqs. (2.3) and (2.4c)
κ	= $(1/\tau)$ × yaw growth per radian of nutation
κ_p	= 0 for $\lambda_k \neq 0$, = 1 for $\lambda_k = 0$ (Eqs. (2.23) of Reference 1)
θ	polar angle (azimuthal coordinate) in inertial system
λ_k	eigenvalue in axial problem, Eqs. (2.6) and (2.7)

μ_j	eigenvalues occurring in series given by the 3rd terms of the right-hand sides of Eq. (2.6); see paragraph preceding Eq. (2.8)
ν	kinematic viscosity of liquid [cm^2/s]
$\tilde{\xi}$	vector describing angular motion of cylinder, Eqs. (1.1) and (1.2)
ρ	density of liquid [g/cm^3]
τ	nutational frequency of cylinder/$\dot{\phi}$
$\dot{\phi}$	spin rate of cylinder [rad/s], taken to be positive
$\psi(r)$	function defined in Eq. (2.17e), used in Eq. (2.16)

DISTRIBUTION LIST

No. of Copies	Organization
12	Administrator Defense Technical Information Center ATTN: DTIC-DDA Cameron Station Alexandria, VA 22314
1	Commander US Army Materiel Command ATTN: AMCDRA-ST 5001 Eisenhower Avenue Alexandria, VA 22333
1	HQDA DAMA-ART-M Washington, DC 20310
1	Commander US Army Engineer Waterways Experiment Station ATTN: R.H. Malter P.O. Box 631 Vicksburg, MS 39180
1	Commander Armament R&D Center US Army AMCCOM ATTN: SMCAR-TDC Dover, NJ 07801
1	Commander Armament R&D Center US Army AMCCOM ATTN: SMCAR-TSS Dover, NJ 07801-5001
6	Commander Armament R&D Center US Army AMCCOM ATTN: SMCAR-LCA-F Mr. D. Mertz Mr. E. Falkowski Mr. A. Loeb Mr. R. Kline Mr. S. Kahn Mr. S. Wasserman Dover, NJ 07801
1	Commander US Army Armament Munitions and Chemical Command ATTN: AMSMC-ESK-L Rock Island, IL 61299
1	Director Benet Weapons Laboratory Armament R&D Center US Army AMCCOM ATTN: SMCAR-LCB-TL Watervliet, NY 12189
1	Commander US Army Aviation Research and Development Command ATTN: AMSAV-E 4300 Goodfellow Blvd St. Louis, MO 63120
1	Director US Army Air Mobility Research and Development Laboratory ATTN: SAVDL-D, W.J. McCroskey Ames Research Center Moffett Field, CA 94035
1	Director US Army Air Mobility Research and Development Laboratory Ames Research Center Moffett Field, CA 94035
1	Commander US Army Communications Research and Development Command ATTN: AMSEL-ATDD Fort Monmouth, NJ 07703
1	Commander US Army Communications and Development Command ATTN: AMSEL-L Fort Monmouth, NJ 07703

DISTRIBUTION LIST

No. of Copies	Organization
1	Commander US Army Electronics Research and Development Command Technical Support Activity ATTN: DELSD-L Fort Monmouth, NJ 07703
1	Commander US Army Missile Command ATTN: AMSMI-YDL Redstone Arsenal, AL 35898
1	Commander US Army Missile Command ATTN: AMSMI-R Redstone Arsenal, AL 35898
1	Commander US Army Missile Command ATTN: AMSMI-RDK, Mr. R. Deep Redstone Arsenal, AL 35898
1	Commander US Army Tank Automotive Command ATTN: AMSTA-TSL Warren, MI 48090
1	Director US Army TRADOC Systems Analysis Activity ATTN: ATAA-SL White Sands Missile Range, NM 88002
1	Commander US Army Jefferson Proving GD Madison, IN 47251
2	Commander US Army Research Office ATTN: Dr. R.E. Singleton Dr. Jagdish Chandra P.O. Box 12211 Research Triangle Park, NC 27709-2211
1	AGARD-NATO APO New York 09777
1	AFWL/SUL Kirtland AFB, NM 87117
1	Commandant US Army Infantry School ATTN: ATSH-CD-CSO-OR Fort Benning, GA 31905
3	Commander Naval Air Systems Command ATTN: AIR-604 Washington, DC 20360
2	Commander David W. Taylor Naval Ship Research & Development Cmd ATTN: H.J. Lugt, Code 1802 S. de los Santos Bethesda, MD 20084
1	Commander Naval Surface Weapons Center ATTN: DX-21, Lib Br Dahlgren, VA 22448
4	Commander Naval Surface Weapons Center Applied Aerodynamics Division ATTN: J.T. Frasier M. Ciment A.E. Winklemann W.C. Ragsdale Silver Spring, MD 20910
1	AFATL (DLJE, Dr. D.C.Daniel) Eglin AFB, FL 32542
2	AFWAL (W.L. Hankey; J.S. Shang) Wright-Patterson AFB, OH 45433
1	Commander US Army Development & Employment Agency ATTN: MODE-TED-SAB Fort Lewis, WA 98433

DISTRIBUTION LIST

No. of Copies	Organization
4	Director National Aeronautics and Space Administration Ames Research Center ATTN: W.C. Rose B. Wick P. Kutler Tech Library Moffett Field, CA 94035
2	Director National Aeronautics and Space Administration Langley Research Center ATTN: Tech Library J. South Langley Station Hampton, VA 23365
1	Director National Aeronautics and Space Administration Lewis Research Center ATTN: MS 60-3, Tech Lib 21000 Brookpark Road Cleveland, OH 44135
2	Director National Aeronautics and Space Administration Marshall Space Flight Center ATTN: A.R. Felix, Chief S&E-AERO-AE Dr. W.W. Fowlis Huntsville, AL 35812
1	AVCO Systems Division ATTN: B. Reeves 201 Lowell Street Wilmington, MA 01887
3	Arnold Research Org., Inc. ATTN: J.D. Whitfield R.K. Matthews J.C. Adams Arnold AFS, TN 37389
3	Aerospace Corporation ATTN: H. Mirels Walter F. Reddall Aerophysics Lab. P.O. Box 92957 Los Angeles, CA 90009
2	Director Jet Propulsion Laboratory ATTN: L.M. Mach Tech Library 4800 Oak Grove Drive Pasadena, CA 91109
3	Boeing Commercial Airplane Company ATTN: R.A. Day, MS 1W-82 P.E. Rubbert, MS 3N-19 J.D. McLean, MS-3N-19 Seattle, WA 98124
3	Calspan Corporation ATTN: G. Homicz P.O. Box 400 Buffalo, NY 14225
1	General Dynamics ATTN: Research Lib 2246 P.O. Box 748 Fort Worth, TX 76101
1	Air Force Armament Laboratory ATTN: AFATL/DLODL Eglin AFB, FL 32542
2	Grumman Aerospace Corporation ATTN: R.E. Melnik L.G. Kaufman Bethpage, NY 11714
2	Lockheed-Georgia Company ATTN: B.H. Little, Jr. G.A. Pounds Dept 72074, Zone 403 86 South Cobb Drive Marietta, GA 30063

DISTRIBUTION LIST

No. of Copies	Organization
1	Lockheed Missiles and Space Company ATTN: Tech Info Center 3251 Hanover Street Palo Alto, CA 94304
3	Martin-Marietta Corporation ATTN: S.H. Maslen S.C. Traugott H. Obremski 1450 S. Rolling Road Baltimore, MD 21227
2	McDonnell Douglas Astronautics Corporation ATTN: J. Xerikos H. Tang 5301 Bolsa Avenue Huntington Beach, CA 92647
1	Douglas Aircraft Company ATTN: T. Cebeci 3855 Lakewood Boulevard Long Beach, CA 90846
3	Rockwell International Science Center ATTN: Dr. V. Shankar Dr. N. Malmuth Dr. S. Chakravarthy 1049 Camino Dos Rios Thousand Oaks, CA 91360
4	Director Sandia National Laboratory ATTN: H.W. Vaughn F.G. Blottner W.L. Oberkampf Tech Lib. Albuquerque, NM 87115
2	United Aircraft Corporation Research Laboratory ATTN: M.J. Werle Library East Hartford, CT 06108
1	Vought Corporation ATTN: J.M. Cooksey, Chief, Gas Dynamics Lab, 2-53700 P.O. Box 5907 Dallas, TX 75222
2	Arizona State University Department of Mechanical and Energy Systems Engineering ATTN: G.P. Neitzel W.S. Saric Tempe, AZ 85287
1	Cornell University Graduate School of Aero Engr ATTN: Library Ithaca, NY 14853
3	California Institute of Technology ATTN: Tech Library H.B. Keller, Math Dept D. Coles, Aero Dept Pasadena, CA 91109
2	Illinois Institute of Tech ATTN: H. M. Nagib, J. Strikwerda 3300 South Federal Chicago, IL 60616
1	The Johns Hopkins University Dept of Mech and Materials Sci. ATTN: S. Corrsin Baltimore, MD 21218
1	University of Tennessee Department of Physics ATTN: Prof. W.E. Scott Knoxville, TN 37916
3	Massachusetts Institute of Technology ATTN: E. Covert H. Greenspan Tech Lib 77 Massachusetts Avenue Cambridge, MA 02139

DISTRIBUTION LIST

No. of Copies	Organization
4	Director Johns Hopkins University Applied Physics Laboratory ATTN: Dr. R.D. Whiting Dr. D.A. Hurdif Dr. R.S. Hirsh Mr. E.R. Bohn Johns Hopkins Road Laurel, MD 20707
2	North Carolina State Univ Mechanical and Aerospace Engineering Department ATTN: F.F. DeJarnette J.C. Williams Raleigh, NC 27607
1	Northwestern University Department of Engineering Science and Applied Mathematics ATTN: Dr. S.H. Davis Evanston, IL 60201
1	Notre Dame University Department of Aero Engr ATTN: T.J. Mueller Notre Dame, IN 46556
2	Ohio State University Dept of Aeronautical and Astronautical Engineering ATTN: S.L. Petrie O.R. Burggraf Columbus, OH 43210
1	Purdue University Thermal Science & Prop Ctr ATTN: Tech Library W. Lafayette, IN 47906
2	Polytechnic Institute of New York ATTN: G. Moretti Tech Library Route 110 Farmingdale, NY 11735
3	Princeton University James Forrestal Research Ctr Gas Dynamics Laboratory ATTN: S.M. Bogdonoff S.I. Cheng Tech Library Princeton, NJ 08540
1	Rensselaer Polytechnic Institute Department of Math Sciences ATTN: Tech Library Troy, NY 12181
1	Rutgers University Department of Mechanical, Industrial, and Aerospace Engineering ATTN: R.H. Page New Brunswick, NJ 08903
1	San Diego State University Department of Aerospace Engr and Engineering Mechanics College of Engineering ATTN: K.C. Wang San Diego, CA 92115
1	Southern Methodist University Department of Civil and Mechanical Engineering ATTN: R.L. Simpson Dallas, TX 75222
1	Southwest Research Institute Applied Mechanics Reviews 8500 Culebra Road San Antonio, TX 78228
2	Stanford University Dept of Aeronautics/Astronautics ATTN: J.L. Steger M. Van Dyke Stanford, CA 94305

DISTRIBUTION LIST

No. of Copies	Organization
1	Texas A&M University College of Engineering ATTN: R.H. Page College Station, TX 77843
1	University of California - Davis ATTN: H.A. Dwyer Davis, CA 95616
1	University of California - Berkeley Department of Aerospace Engineering ATTN: M. Holt Berkeley, CA 94720
2	University of California - San Diego Department of Aerospace Engineering and Mechanical Engineering Sciences ATTN: P. Libby Tech Library La Jolla, CA 92037
1	University of California - Santa Barbara Department of Mechnical and Environmental Engineering ATTN: J.P. Vanyo Santa Barbara, CA 93106
1	University of Colorado Department of Astro-Geophysics ATTN: E.R. Benton Boulder, CO 80302
2	University of Cincinnati Department of Aerospace Engineering ATTN: R.T. Davis S.G. Rubin Cincinnati, OH 45221
2	University of Maryland ATTN: W. Melnik J.D. Anderson College Park, MD 20740
1	University of Maryland - Baltimore County Department of Mathematics ATTN: Dr. Y.M. Lynn 5401 Wilkens Avenue Baltimore, MD 21228
1	University of Santa Clara Department of Physics ATTN: R. Greeley Santa Clara, CA 95053
2	University of Southern California Department of Aerospace Engineering ATTN: T. Maxworthy P. Weidman Los Angeles, CA 90007
2	University of Michigan Department of Aeronautical Engineering ATTN: W.W. Wilmarth Tech Library East Engineering Building Ann Arbor, MI 48104
2	University of Rochester Department of Mechanical and Aerospace Sciences ATTN: R. Gans A. Clark, Jr. Rochester, NY 14627

DISTRIBUTION LIST

No. of Copies	Organization
1	University of Texas Department of Aerospace Engineering ATTN: J.C. Westkaemper Austin, TX 78712
3	University of Virginia Department of Mechanical Aerospace Engineering ATTN: W.G. Wood R.J. Ribando R. Krauss Charlottesville, VA 22904
1	University of Washington Department of Mechanical Engineering ATTN: Tech Library Seattle, WA 98105
1	University of Wyoming ATTN: D.L. Boyer University Station Laramie, WY 82071
1	U.S. Military Academy Department of Physics ATTN: MAJ G. Heuser West Point, NY 10996
1	Woods Hole Oceanographic Institute ATTN: J.A. Whitehead Woods Hole, MA 02543
2	Virginia Polytechnic Institute and State University Department of Aerospace Engineering ATTN: Tech Library Dr. T. Herbert Blacksburg, VA 24061

Aberdeen Proving Ground

Director, USAMSAA
ATTN: AMXSY-D
AMXSY-MP, H. Cohen

Commander, USATECOM
ATTN: AMSTE-TO-F

Commander, CRDC, AMCCOM
ATTN: SMCCR-RSP-A
W. C. Dee
SMCCR-MU
M. C. Miller
ATTN: SMCCR-RSP-A
SMCCR-MU
SMCCR-SPS-IL

USER EVALUATION SHEET/CHANGE OF ADDRESS

This Laboratory undertakes a continuing effort to improve the quality of the reports it publishes. Your comments/answers to the items/questions below will aid us in our efforts.

1. BRL Report Number _____ Date of Report _____

2. Date Report Received _____

3. Does this report satisfy a need? (Comment on purpose, related project, or other area of interest for which the report will be used.) _____

_____

_____

4. How specifically, is the report being used? (Information source, design data, procedure, source of ideas, etc.) _____

_____

_____

5. Has the information in this report led to any quantitative savings as far as man-hours or dollars saved, operating costs avoided or efficiencies achieved etc? If so, please elaborate. _____

_____

_____

6. General Comments. What do you think should be changed to improve future reports? (Indicate changes to organization, technical content, format, etc.)

_____

_____

_____

CURRENT ADDRESS

_____
Name

_____
Organization

_____
Address

_____
City, State, Zip

7. If indicating a Change of Address or Address Correction, please provide the New or Correct Address in Block 6 above and the Old or Incorrect address below.

OLD ADDRESS

_____
Name

_____
Organization

_____
Address

_____
City, State, Zip

(Remove this sheet along the perforation, fold as indicated, staple or tape closed, and mail.)

FOLD HERE

Director
US Army Ballistic Research Laboratory
ATTN: AMXBR-OD-ST
Aberdeen Proving Ground, MD 21005-5066

NO POSTAGE
NECESSARY
IF MAILED
IN THE
UNITED STATES

OFFICIAL BUSINESS
PENALTY FOR PRIVATE USE. $300

BUSINESS REPLY MAIL
FIRST CLASS PERMIT NO 12062 WASHINGTON, DC
POSTAGE WILL BE PAID BY DEPARTMENT OF THE ARMY

Director
US Army Ballistic Research Laboratory
ATTN: AMXBR-OD-ST
Aberdeen Proving Ground, MD 21005-9989

FOLD HERE

END

FILMED

3-85

DTIC